Two-proton radioactivity and three-body decay. III. Integral formulas for decay widths in a simplified semianalytical approach

L. V. Grigorenko[1,2,3] and M. V. Zhukov[4]
[1]*Flerov Laboratory of Nuclear Reactions, JINR, RU-141980 Dubna, Russia*
[2]*Gesellschaft für Schwerionenforschung mbH, Planckstrasse 1, D-64291 Darmstadt, Germany*
[3]*RRC "The Kurchatov Institute", Kurchatov sq. 1, RU-123182 Moscow, Russia*
[4]*Fundamental Physics, Chalmers University of Technology, S-41296 Göteborg, Sweden*
(Received 10 April 2007; published 30 July 2007)

Three-body decays of resonant states are studied using integral formulas for decay widths. The theoretical approach with a simplified Hamiltonian allows semianalytical treatment of the problem. The model is applied to decays of the first excited $3/2^-$ state of ^{17}Ne and the $3/2^-$ ground state of ^{45}Fe. The convergence of three-body hyperspherical model calculations to the exact result for widths and energy distributions are studied. The theoretical results for ^{17}Ne and ^{45}Fe decays are updated, and uncertainties of the derived values are discussed in detail. Correlations for the decay of the ^{17}Ne $3/2^-$ state are also studied.

DOI: 10.1103/PhysRevC.76.014008 PACS number(s): 21.60.Gx, 21.45.+v, 23.50.+z, 21.10.Tg

I. INTRODUCTION

The idea of a "true" two-proton radioactivity was proposed about 50 years ago in the classical paper of Goldansky [1]. The word "true" denotes here that we are dealing not with a relatively simple emission of two protons, which becomes possible in every nucleus above the two-proton decay threshold, but with a specific situation in which one-proton emission is prohibited either energetically (because of the proton separation energy in the daughter system) or dynamically (because of various factors). Only the simultaneous emission of two protons is possible in that case (see Fig. 1; more details on the modes of three-body decays can be found in Ref. [2]). The dynamics of such decays cannot be reduced to a sequence of two-body decays, and from a theoretical point of view we have to deal with a three-body Coulomb problem in the continuum, which is known to be very complicated.

Progress in this field has been quite slow. Only recently, a consistent quantum mechanical theory of the process was developed [2–4], which allows one to study the two-proton (three-body) decay phenomenon in a three-body cluster model. It has been applied to a range of a light nuclear systems (^{12}O, ^{16}Ne [5], ^{6}Be, ^{8}Li*,^{9}Be* [6], ^{17}Ne*,^{19}Mg [7]). Systematic exploratory studies of the heavier prospective $2p$ emitters ^{30}Ar, ^{34}Ca, ^{45}Fe, ^{48}Ni, ^{54}Zn, ^{58}Ge, ^{62}Se, and ^{66}Kr [4,8] have provided predictions of lifetime ranges and possible correlations among fragments.

Experimental studies of the two-proton radioactivity is presently an actively developing field. Since the first experimental identification of $2p$ radioactivity in ^{45}Fe [9,10], it has also been found in ^{54}Zn [11]. Some fingerprints of the ^{48}Ni $2p$ decay have been observed, and the ^{45}Fe lifetime and decay energy have been measured with improved accuracy [12]. There was an intriguing discovery of the extreme enhancement of the $2p$ decay mode for the high-spin 21^+ isomer of ^{94}Ag, interpreted so far only in terms of the hyperdeformation of this state [13]. New experiments aimed at more detailed $2p$ decay studies (e.g., the observation of correlations) are under way at Gesellschaft für Schwerionenforschung (GSI) (^{19}Mg), Michigan State University (MSU) (^{45}Fe), Grand Accelerateur National D'Ions Lourds (GANIL) (^{45}Fe), and the University of Jyväskylä (^{94}Ag).

Several other theoretical approaches have been applied to the problem in recent years. We should mention the diproton model [14,15], R-matrix approach [16–19], continuum shell model [20], and adiabatic hyperspherical approach [21]. Some issues of a compatibility between different approaches will be addressed in this work and in the companion paper [22].

Another, possibly very important, field of application of the two-proton decay studies was shown in Refs. [23,24]. It was demonstrated in Ref. [23] that the importance of direct resonant two-proton radiative capture processes was underestimated in earlier treatment of the rp-process waiting points [25]. The scale of modification of the astrophysical $2p$ capture rates can be as large as several orders of magnitude in certain temperature ranges. In paper [24] it was found that nonresonant $E1$ contributions to three-body (two-proton) capture rates can also be much larger than was expected before. The updated $2p$ astrophysical capture rate for the ^{15}O$(2p,\gamma)^{17}$Ne reaction appears to be competing with the standard ^{15}O$(\alpha,\gamma)^{19}$Ne breakout reaction for the hot carbon-nitrogen-oxygen (CNO) cycle. The improvements of the $2p$ capture rates obtained in Refs. [23,24] are connected to consistent quantum mechanical treatment of the three-body Coulomb continuum in contrast to the essentially quasiclassical approach typically used in astrophysical calculations of three-body capture reactions (e.g., [25,26]).

The growing quality of the experimental studies of the $2p$ decays and the high precision required for certain astrophysical calculations inspired us to revisit the issues connected with the various uncertainties and technical difficulties of our studies. In this work, we perform the following: (i) We extend the two-body formalism of the integral formulas for width to the three-body case. We perform the relevant derivations for the two-body case to make the necessary approximations and assumptions explicit. (ii) We formulate a simplified three-body model which has many dynamical features similar to the

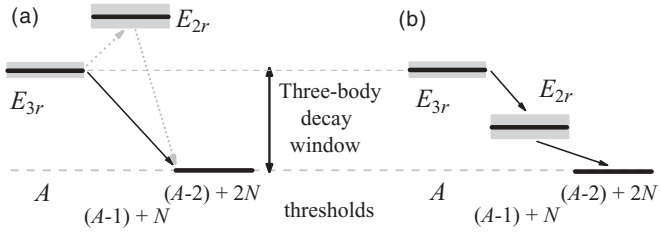

FIG. 1. Energy conditions for different modes of the two-nucleon emission (three-body decay): (a) true three-body decay, (b) sequential decay.

realistic case, but allows the exact semianalytical treatment and thus makes possible a precise calibration of three-body calculations. It is also possible to study in detail several important dependencies of three-body widths in the frame of this model. (iii) We perform practical studies of some systems of interest and demonstrate a connection between the simplified semianalytical formalism and the realistic three-body calculations.

The unit system $\hbar = c = 1$ is used in the article.

II. INTEGRAL FORMULA FOR WIDTH

Integral formalisms of width calculations for narrow two-body states have been known for a long time, e.g., see Refs. [27,28]. The prime objective of those studies was α-decay widths. An interesting overview of this field can be found in Ref. [29]. This approach, in our opinion, did not produce novel results as the inherent uncertainties of the method are essentially the same as those of the R-matrix phenomenology, which is technically much simpler (see, e.g., a discussion in Ref. [30]). An important nontrivial application of the integral formalism was the calculation of widths for proton emission off deformed states [31,32]. There were attempts to extend the integral formalism to the three-body decays, using a formal generalization for the hyperspherical space [2,33]. These were shown to be difficult with respect to technical realization and inferior to other methods developed in Refs. [2,3].

Here we develop an integral formalism for the three-body (two-proton) decay width in a different way. However, first we review the standard formalism to define (more clearly) the approximations used.

A. Width definition, complex energy wave function

For decay studies we consider the wave function (WF) with complex pole energy

$$\tilde{E}_r = \tilde{k}_r^2/(2M) = E_r - i\Gamma/2, \quad \tilde{k}_r \approx k_r - i\Gamma/(2v_r),$$

where $v = \sqrt{2E/M}$. The pole solution for the Hamiltonian

$$(H - \tilde{E}_r)\Psi_{lm}^{(+)}(\mathbf{r}) = (T + V - \tilde{E}_r)\Psi_{lm}^{(+)}(\mathbf{r}) = 0$$

provides the WF with the outgoing asymptotic

$$\Psi_{lm}^{(+)}(\mathbf{r}) = r^{-1}\psi_l^{(+)}(kr)Y_{lm}(\hat{r}). \tag{1}$$

For the single-channel two-body problem, the pole solution is formed only for one selected value of angular momentum l. In the asymptotic region,

$$\psi_l^{(+)}(\tilde{k}_r r) \overset{r\geq R}{=} H_l^{(+)}(\tilde{k}_r r) = G_l(\tilde{k}_r r) + iF_l(\tilde{k}_r r). \tag{2}$$

The above asymptotic is growing exponentially

$$\psi_l^{(+)}(\tilde{k}_r r) \overset{r>R}{\sim} \exp[+i\tilde{k}_r r] \approx \exp[+ik_r r]\exp[+\Gamma r/(2v_r)]$$

as a function of the radius at pole energy. This unphysical growth is connected to the use of time-independent formalism and could be reliably neglected for the typical *radioactivity* time scale as it has a noticeable effect at very large distances.

Applying Green's procedure to the complex energy WF

$$\Psi^{(+)\dagger}[(H - \tilde{E}_r)\Psi^{(+)}] - [(H - \tilde{E}_r)\Psi^{(+)}]^\dagger\Psi^{(+)} = 0,$$

we get for the partial components at pole energy $\tilde{E}_r$

$$i\Gamma\psi_l^{(+)*}\psi_l^{(+)} = \frac{1}{2M}\left[\psi_l^{(+)*}\frac{d^2\psi_l^{(+)}}{dr^2} - \frac{d^2\psi_l^{(+)*}}{dr^2}\psi_l^{(+)}\right].$$

After radial integration from 0 to R (here and below, R denotes the radius sufficiently large that the nuclear interaction disappears), we obtain

$$\Gamma = \frac{\left[\psi_l^{(+)*}\left(\frac{d}{dr}\psi_l^{(+)}\right) - \left(\frac{d}{dr}\psi_l^{(+)*}\right)\psi_l^{(+)}\right]\Big|_{r=R}}{2Mi\int_0^R \left|\psi_l^{(+)}\right|^2 dr} = \frac{j_l}{N_l}, \tag{3}$$

which corresponds to a definition of the width as a decay probability (reciprocal of the lifetime):

$$N = N_0\exp[-t/\tau] = N_0\exp[-\Gamma t].$$

The width Γ is then equal to the outgoing flux j_l through the sphere of sufficiently large radius R, divided by the number of particles N_l inside the sphere.

Using Eq. (2), the flux in the asymptotic region could be rewritten for $\tilde{k}_r \to k_r$ in terms of a Wronskian, that is,

$$\begin{aligned} j_l &= \frac{1}{2Mi}\left[\psi_l^{(+)*}\left(\frac{d}{dr}\psi_l^{(+)}\right) - \left(\frac{d}{dr}\psi_l^{(+)*}\right)\psi_l^{(+)}\right]\Big|_{r=R} \\ &= (k_r/M)W(F_l(k_r R), G_l(k_r R)) = v_r, \end{aligned} \tag{4}$$

where the Wronskian for the real energy functions F_l, G_l is

$$W(F_l, G_l) = G_l F_l' - G_l' F_l \equiv 1.$$

The effect of the complex energy is easy to estimate (actually without loss of a generality) in a small energy approximation

$$F_l(kr) \overset{kr\to 0}{\sim} C_l(kr)^{l+1}, \quad G_l(kr) \overset{kr\to 0}{\sim} \frac{(kr)^{-l}}{(2l+1)C_l}, \tag{5}$$

where C_l is a Coulomb coefficient (defined, e.g., in Ref. [34]). The flux is then

$$\begin{aligned} j_l &= \frac{\tilde{k}_r H_l^{(-)}(\tilde{k}_r^* r)H_l^{(+)\prime}(\tilde{k}_r r) - \tilde{k}_r^* H_l^{(-)\prime}(\tilde{k}_r^* r)H_l^{(+)}(\tilde{k}_r r)}{2iM} \\ &= v_r\left(1 - \frac{2l(l+1)}{k_r^2}\left(\frac{\Gamma}{2v_r}\right)^2 + l \times o[\Gamma^3]\right). \end{aligned}$$

So, the equality (4) is always valid for $l = 0$, and for $l \neq 0$ we get

$$\Gamma \ll \left(\frac{8}{l(l+1)}\right)^{1/2} E_r.$$

B. Two-body case, real energy WF

Now we need a WF for the real energy $E = k^2/2M$ solution of the Schrödinger equation

$$(H - E)\Psi_{\mathbf{k}}(\mathbf{r}) = (T + V^{\text{nuc}} + V^{\text{coul}} - E)\Psi_{\mathbf{k}}(\mathbf{r}) = 0,$$
$$\Psi_{\mathbf{k}}(\mathbf{r}) = 4\pi \sum\nolimits_l i^l (kr)^{-1}\psi_l(kr) \sum\nolimits_m Y^*_{lm}(\hat{k})Y_{lm}(\hat{r}),$$

in the S-matrix representation, which means that for $r > R$,

$$\psi_l(kr) = \frac{i}{2}[(G_l(kr) - iF_l(kr)) - S_l(G_l(kr) + iF_l(kr))].$$

At resonance energy E_r,

$$S_l(E_r) = e^{2i\delta_l(E_r)} = e^{2i\pi/2} = -1,$$

and in the asymptotic region, defined by the maximal size of the nuclear interaction R,

$$\psi_l(k_r r) \overset{r\geq R}{=} iG_l(k_r r).$$

At resonance energy, we can define a "quasibound" WF $\tilde{\psi}_l$ as matching the irregular solution G_l and normalized to unity for the integration in the internal region limited by radius R:

$$\tilde{\psi}_l(k_r r) = \frac{(-i)\psi_l(k_r r)}{\left(\int_0^R |\psi_l(k_r x)|^2 dx\right)^{1/2}} = -i\frac{\psi_l(k_r r)}{N_l{}^{1/2}}. \quad (6)$$

Now we introduce an auxiliary Hamiltonian $\bar{H}$ with different short range nuclear interaction $\bar{V}^{\text{nuc}}$,

$$(\bar{H} - E)\Phi_{\mathbf{k}}(\mathbf{r}) = (T + \bar{V}^{\text{nuc}} + V^{\text{coul}} - E)\Phi_{\mathbf{k}}(\mathbf{r}) = 0,$$

and also construct the other WF in an S-matrix representation

$$\Phi_{\mathbf{k}}(\mathbf{r}) = 4\pi \sum\nolimits_l i^l (kr)^{-1}\varphi_l(kr) \sum\nolimits_m Y^*_{lm}(\hat{k})Y_{lm}(\hat{r}),$$
$$\varphi_l(kr) = \frac{i}{2}[(G_l(kr) - iF_l(kr)) - \bar{S}_l(G_l(kr) + iF_l(kr))],$$

for $r > R$. Or in the equivalent form

$$\varphi_l(kr) = \exp(i\bar{\delta}_l)[F_l(kr)\cos(\bar{\delta}_l) + G_l(kr)\sin(\bar{\delta}_l)]. \quad (7)$$

The Hamiltonian $\bar{H}$ should provide the WF $\Phi_{\mathbf{k}}(\mathbf{r})$ which at energy E_r is sufficiently far from being a resonance WF; therefore, for this WF $\bar{\delta}_l(E_r) \sim 0$.

For real energy WFs $\Psi_{\mathbf{k}}(\mathbf{r})$ and $\Phi_{\mathbf{k}}(\mathbf{r})$, we can write

$$\Phi_{\mathbf{k}}(\mathbf{r})^\dagger[(H - E)\Psi_{\mathbf{k}}(\mathbf{r})] - [(\bar{H} - E)\Phi_{\mathbf{k}}(\mathbf{r})]^\dagger\Psi_{\mathbf{k}}(\mathbf{r}) = 0,$$
$$\varphi^*_l(V - \bar{V})\psi_l = \frac{1}{2M}\left[\varphi^*_l\left(\frac{d^2}{dr^2}\psi_l\right) - \left(\frac{d^2}{dr^2}\varphi^*_l\right)\psi_l\right]. \quad (8)$$

For WFs taken at resonance energy E_r, this expression provides

$$2M\int_0^R \varphi^*_l(V - \bar{V})\psi_l dr = 2MiN_l{}^{1/2}\int_0^R \varphi^*_l(V - \bar{V})\tilde{\psi}_l dr$$
$$= \exp(-i\bar{\delta}_l)\cos(\bar{\delta}_l)k_r W(F_l(k_r R),$$
$$\times G_l(k_r R)),$$
$$N_l{}^{1/2} = \frac{-i\exp(-i\bar{\delta}_l)\cos(\bar{\delta}_l)k_r}{2M\int_0^R \varphi^*_l(V - \bar{V})\tilde{\psi}_l dr}. \quad (9)$$

From Eqs. (3), (4), and (6) and the approximation $\psi^{(+)}_l \approx \psi_l$, it follows that

$$\Gamma = \frac{v_r}{\int_0^R |\psi^{(+)}_l|^2 dr} \approx \frac{v_r}{\int_0^R |\psi_l|^2 dr} = \frac{v_r}{|N_l^{1/2}|^2},$$
$$\Gamma = \frac{4}{v_r\cos^2(\bar{\delta}_l)}\left|\int_0^R \varphi^*_l(V - \bar{V})\tilde{\psi}_l dr\right|^2. \quad (10)$$

So, the idea of the integral method is to define the internal normalizations for the WF with resonant boundary conditions (this is equivalent to determining the outgoing flux for a normalized "quasibound" WF) by the help of the eigenfunction of the auxiliary Hamiltonian $\bar{H}$, which has the same long-range behavior and differs only in the compact region.

III. ALTERNATIVE DERIVATION

Let us reformulate the derivation of Eq. (10) in a more general way, so that the detailed knowledge of the WF structure for ψ_l and $\psi^{(+)}_l$ is not required. It would allow a straightforward extension of the formalism to the three-body case. We start from the Schrödinger equation in continuum with solution $\Psi^{(+)}$ at the pole energy $\tilde{E}_r = E_r + i\Gamma/2$:

$$(H - \tilde{E}_r)\Psi^{(+)} = (T + V - \tilde{E}_r)\Psi^{(+)} = 0. \quad (11)$$

Then we rewrite it identically via the auxiliary Hamiltonian $\bar{H} = T + \bar{V}$

$$(H + \bar{V} - V - \tilde{E}_r)\Psi^{(+)} = (\bar{V} - V)\Psi^{(+)},$$
$$(\bar{H} - E_r)\Psi^{(+)} = (\bar{V} - V + i\Gamma/2)\Psi^{(+)}. \quad (12)$$

Thus we can use the real energy Green's function $\bar{G}_{E_r}$ of auxiliary Hamiltonian $\bar{H}$ to "regenerate" the WF with the outgoing asymptotic

$$\bar{\Psi}^{(+)} = \bar{G}^{(+)}_{E_r}(\bar{V} - V + i\Gamma/2)\Psi^{(+)}. \quad (13)$$

At this point in Eq. (13), $\bar{\Psi}^{(+)} \equiv \Psi^{(+)}$ and the bar in the notation for the "corrected" WF $\bar{\Psi}^{(+)}$ is introduced for later use to distinguish it from the "initial" WF $\Psi^{(+)}$ [the one before application of Eq. (13)]. Further assumptions we should consider separately in two-body and three-body cases.

A. Two-body case

To define the width Γ by Eq. (3) we need to know the complex energy solution $\Psi^{(+)}$ at pole energy. For narrow states $\Gamma \ll E_r$, this solution can be obtained in a simplified way using the following approximations.

(i) For narrow states, we can always choose the auxiliary Hamiltonian in such a way that $\Gamma \ll \bar{V} - V$, and we can assume $\Gamma \to 0$ in the Eq. (13).

(ii) Instead of a complex energy solution $\Psi^{(+)}$ in the right-hand side of Eq. (13), we can use the normalized real energy quasibound solution $\tilde{\Psi}$ defined for one real resonant value of energy $E_r = k_r^2/2M$, that is,

$$N_l = \int d\Omega \int_0^R dr r^2 |\tilde{\Psi}_{lm}(\mathbf{r})|^2 \equiv 1.$$

So, Eq. (13) is used in the form

$$\bar{\Psi}^{(+)}_{lm} = \bar{G}^{(+)}_{E_r}(\bar{V} - V)\tilde{\Psi}_{lm}. \tag{14}$$

The solution $\bar{\Psi}^{(+)}$ is matched to the function

$$h^{(+)}_l(kr) = G_l(kr) + iF_l(kr), \tag{15}$$

while the solution $\tilde{\Psi}$ is matched to the function G_l. For deep-subbarrier energies, it is reasonable to expect that in the internal region $r \leqslant R$,

$$G_l \gg F_l \rightarrow \|\mathrm{Re}[\tilde{\Psi}^{(+)}]\| \approx \|\tilde{\Psi}\| \gg \|\mathrm{Im}[\tilde{\Psi}^{(+)}]\|,$$

where tildes denote that WFs are normalized in the internal region. In the single-channel case, it can be shown by direct calculation that an approximate equality

$$\frac{MR^2\Gamma}{\pi}\|\mathrm{Re}[\tilde{\Psi}^{(+)}]\| \gtrsim \|\mathrm{Im}[\tilde{\Psi}^{(+)}]\|$$

holds in the internal region, and thus for narrow states $\Gamma \ll E_r$, the approximation (13) $\rightarrow$ (14) should be very reliable.

To derive Eq. (10), the WF with an outgoing asymptotic is generated using the Green's function of the auxiliary Hamiltonian $\bar{H}$ and the "transition potential" $(V - \bar{V})$. The standard two-body Green's function is

$$\bar{G}^{(+)}_{k^2/(2m)}(\mathbf{r},\mathbf{r}') = \frac{2M}{krr'}\sum_l \left\{ \begin{array}{ll} \varphi_l(kr)h^{(+)}_l(kr'), & r \leqslant r' \\ h^{(+)}_l(kr)\varphi_l(kr'), & r > r' \end{array} \right\} \times \sum\nolimits_m Y_{lm}(\hat{r})Y^*_{lm}(\hat{r}'), \tag{16}$$

where the radial WFs $h^{(+)}_l$ and φ_l of the auxiliary Hamiltonian are defined in Eqs. (15) and (7).

$$\bar{\Psi}^{(+)}_{lm}(\mathbf{r}) = \int d\mathbf{r}'\bar{G}^{(+)}_{k^2/(2m)}(\mathbf{r},\mathbf{r}')(\bar{V} - V)\tilde{\Psi}_{l'm'}(\mathbf{r}').$$

For the asymptotic region $r > R$,

$$\bar{\Psi}^{(+)}_{lm}(\mathbf{r}) = \frac{2M}{k_r r}h^{(+)}_l(k_r r)Y_{lm}(\hat{r}) \times \int_0^R dr'\varphi_l(k_r r')(\bar{V} - V)\tilde{\psi}_l(k_r, r').$$

The outgoing flux is then calculated [see Eq. (4)]

$$j_l = \frac{R^2}{2l+1}\sum_m \int d\Omega \frac{1}{M}\mathrm{Im}\left[\bar{\Psi}^{(+)*}_{lm}(\mathbf{r})\nabla\bar{\Psi}^{(+)}_{lm}\right]\Big|_{r=R}.$$

As far as function $\tilde{\Psi}$ is normalized by construction, then

$$\Gamma \equiv j_l = \frac{4}{v_r}\left|\int_0^R dr\varphi_l(k_r r)(\bar{V} - V)\tilde{\psi}_l(k_r, r)\right|^2. \tag{17}$$

Note, that this equation differs from Eq. (10) only by a factor of $1/(\cos^2[\bar{\delta}_l])$ which should be very close to unity for sufficiently high barriers.

B. Simplified model for three-body case

In papers [2,3], the widths for three-body decays were defined by the following procedure. We solve numerically the three-body problem

$$(H - E_{3r})\tilde{\Psi} = 0.$$

The equation is solved using the hyperspherical harmonic (HH) method with *some* box boundary conditions (e.g., zero or quasibound in diagonal channels at large distances) getting the WF $\tilde{\Psi}$ (normalized in the finite domain) and the value of the real resonant energy E_{3r}. Thereupon we search for the outgoing solution $\Psi^{(+)}$ of the equation

$$(H - E_{3r})\Psi^{(+)} = -i\Gamma/2\tilde{\Psi}$$

with the approximate boundary conditions of a three-body Coulomb problem (see Ref. [2] for details) and arbitrary Γ. The width is then defined as the flux through the hypersphere of the large radius divided by normalization within this radius:

$$\Gamma = \frac{j}{N} = \frac{\int d\Omega_5\ \Psi^{(+)*}\rho^{5/2}\frac{d}{d\rho}\rho^{5/2}\Psi^{(+)}\Big|_{\rho=\rho_{\max}}}{M\int d\Omega_5 \int_0^{\rho_{\max}}\rho^5 d\rho|\Psi^{(+)}|^2}. \tag{18}$$

The three-body WF with outgoing asymptotic is

$$\Psi^{(+)}_{JM}(\rho,\Omega_5) = \rho^{-5/2}\sum\nolimits_{K\gamma}\chi^{(+)}_{K\gamma}(\rho)\mathcal{J}^{JM}_{K\gamma}(\Omega_5), \tag{19}$$

where the definitions of the hyperspherical variables ρ, Ω_5 and hyperspherical harmonics $\mathcal{J}^{JM}_{K\gamma}$ can be found in Ref. [4].

Here we formulate the simplified three-body model in the way which, on one hand, keeps the important dynamical features of the three-body decays (typical sizes of the nuclear potentials, typical energies in the subsystems, correct ratios of masses, etc.), and, on the other hand, allows a semianalytical treatment of the problem. Two types of approximations are made here.

The three-body Coulomb interaction is

$$V^{\mathrm{coul}} = \frac{Z_1Z_2\alpha}{X} + \frac{Z_1Z_3\alpha}{\left|\mathbf{Y} + \frac{A_2\mathbf{X}}{A_1+A_2}\right|} + \frac{Z_2Z_3\alpha}{\left|\mathbf{Y} - \frac{A_1\mathbf{X}}{A_1+A_2}\right|}, \tag{20}$$

where α is the fine structure constant. By convention, see, e.g., Fig. 2, in the "T" Jacobi system, the core is particle number 3 and in the "Y" system it is particle number 2. We assume that the above potential can be approximated by Coulomb terms which depend on Jacobi variables X and Y only, that is,

$$V^{\mathrm{coul}}_x(X) = \frac{Z_x\alpha}{X}, \quad V^{\mathrm{coul}}_y(Y) = \frac{Z_y\alpha}{Y},$$

(in reality for small X and Y values, the Coulomb form factors of the homogeneously charged sphere with radius r_{sph}

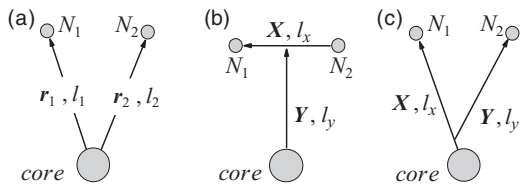

FIG. 2. Single-particle coordinate systems: (a) V system typical for a shell model. (b) T Jacobi system, where the diproton and core are explicitly in configurations with definite angular momenta l_x and l_y. (c) Y Jacobi system, which for a heavy core, is close to the single-particle system (a).

are always used). The effective charges Z_x and Z_y could be considered in two ways.

(i) We can neglect one of the Coulomb interactions. This approximation is consistent with the physical situation of a heavy core and treatment of two final state interactions. Such a situation presumes that the Y Jacobi system is preferable and there is a symmetry in the treatment of the X and Y coordinates, which are close to shell-model single-particle coordinates:

$$Z_x = Z_1 Z_{\rm core}, \quad Z_y = Z_2 Z_{\rm core}. \tag{21}$$

Further we refer to this approximation as the "no p-p Coulomb" case, as typically the proton-proton Coulomb interaction is neglected compared to the Coulomb interaction of a proton with a heavy core.

(ii) We can also consider two particles on the X coordinate as one single particle. The Coulomb interaction in the p-p channel is thus somehow taken into account effectively via a modification of the Z_y charge:

$$Z_x = Z_1 Z_{\rm core}, \quad Z_y = Z_2 (Z_{\rm core} + Z_1). \tag{22}$$

Below we call this situation the "effective p-p Coulomb" case.

For nuclear interactions, we can make the following assumptions:

(i) There is only one nuclear pairwise interaction and

$$\begin{aligned} H &= T + V_3(\rho) + V_x^{\rm coul}(X) \\ &\quad + V_x^{\rm nuc}(X) + V_y^{\rm coul}(Y), \\ \Delta V(X,Y) &= V_y^{\rm nuc}(Y) - V_3(\rho). \end{aligned} \tag{23}$$

This approximation is good for methodological purposes, as it allows us to focus on one degree of freedom and isolate it from the others. From a physical point of view, it could be reasonable if only one FSI is strong,[1] or we have reason to think that the decay mechanism associated with this particular FSI is dominating. Potential $V_y^{\rm nuc}(Y)$ in the auxiliary Hamiltonian (27) is "unphysical" in that case and can be put to zero.[2] We further refer to this model as "one final state interaction" (OFSI).

(ii) We can consider two final state interactions (TFSI). A simple form of Green's function in that case can be preserved only if the core mass is considered as infinite (the X and Y coordinates in the Y Jacobi system coincide with single-particle core-p coordinates). In that case, both pairwise interactions $V_x^{\rm nuc}(X)$ and $V_y^{\rm nuc}(Y)$ are treated as "physical," which means that they are both present in the initial and in the auxiliary Hamiltonians. Thus only the three-body potential "survives" the $\bar{V} - V$ subtraction:

$$\begin{aligned} H &= T + V_3(\rho) + V_x^{\rm coul}(X) + V_x^{\rm nuc}(X) \\ &\quad + V_y^{\rm coul}(Y) + V_y^{\rm nuc}(Y), \\ \Delta V(X,Y) &= -V_3(\rho). \end{aligned} \tag{24}$$

The three-body potential is used in this work in the Woods-Saxon form

$$V_3(\rho) = V_3^0 (1 + \exp[(\rho - \rho_0)/a_\rho])^{-1}, \tag{25}$$

with $\rho_0 = 5$ fm for ^{17}Ne, $\rho_0 = 6$ fm for ^{45}Fe,[3] and a small value of diffuseness parameter $a_\rho = 0.4$ fm. Use of such three-body potential is an important difference from our previous calculations, where it was utilized in the form

$$V_3(\rho) = V_3^0 (1 + (\rho/\rho_0)^3)^{-1}, \tag{26}$$

which provides the long-range behavior $\sim\rho^{-3}$. Such an asymptotic in the ρ variable is produced by short-range pairwise nuclear interactions, and thus the interpretation of three-body potential (26) is phenomenological taking into account those components of pairwise interactions which were omitted for some reason in the calculations. In this work, the aim of the potential V_3 is different. On the one hand, we would like to keep the three-body energy fixed while varying the properties (and number) of pairwise interactions. On the other hand, we do not want to change the properties of the Coulomb barriers beyond the typical nuclear distance (this is achieved by the small diffuseness of the potential). Thus the potential (25) is phenomenological taking into account interactions that act only when both valence nucleons are close to the core (both move in the mean field of the nucleus).

The auxiliary Hamiltonian is taken in the form that allows a separate treatment of X and Y variables, that is,

$$\bar{H} = T + V_x^{\rm coul}(X) + V_x^{\rm nuc}(X) + V_y^{\rm coul}(Y) + V_y^{\rm nuc}(Y). \tag{27}$$

In this formulation of the model, the Coulomb potentials are fixed as shown above. The nuclear potential $V_x^{\rm nuc}(X)$ [and $V_y^{\rm nuc}(Y)$ if present] defines the position of the state in the X [and Y] subsystem. The three-body potential $V_3(\rho)$ defines the position of the three-body state, which is found using the three-body HH approach of Refs. [2,4]. After that, a new WF with outgoing asymptotic is generated by means of the three-body Green's function which can be written for Eq. (27) in a factorized form (without paying attention to the angular

[1] A realistic example of this situation is the case of "E1" (coupled to the ground state by the E1 operator) continuum considered in Ref. [24]. This case is relevant to the low energy radiative capture reactions, important for astrophysics, but deal with nonresonant continuum only.

[2] An interesting numerical stability test is a variation of the unphysical (for OFSI approximation) potential $V_y^{\rm nuc}(Y)$ in the auxiliary Hamiltonian (27). It can be used for numerical tests of the procedure as it should not influence the width. Really, for variation of this potential from weak attraction (we should not allow an unphysical resonance into the decay window) to strong repulsion (scale of the variation is tens of MeV for potential with some typical radius) the width is varied only within a couple of percents. This shows high numerical stability of the procedure.

[3] These values can be evaluated as a typical nuclear radius (here potential radius) for the system multiplied by $\sqrt{2}$; i.e., $3.53\sqrt{2} \approx 5$ and $4.29\sqrt{2} \approx 6$.

coupling)

$$G^{(+)}_{E_{3r}}(\mathbf{XY},\mathbf{X'Y'}) = \frac{1}{2\pi i}\int_{-\infty}^{\infty} dE_x G^{(+)}_{E_x}(\mathbf{X},\mathbf{X'}) G^{(+)}_{E_y}(\mathbf{Y},\mathbf{Y'}),$$

where $E_{3r} = E_x + E_y$ (E_x, E_x are energies of subsystems). The two-body Green's functions in the expressions above are defined as in Eq. (16) via eigenfunctions of the sub-Hamiltonians

$$\begin{cases} \bar{H}_x - E_x = T_x + V^{\rm coul}_x(X) + V^{\rm nuc}_x(X) - E_x, \\ \bar{H}_y - E_y = T_y + V^{\rm coul}_y(Y) + V^{\rm nuc}_y(Y) - E_y. \end{cases}$$

In the OFSI case, the nuclear potential in the Y subsystem should be $V^{\rm nuc}_y(Y) \equiv 0$. The "corrected" continuum WF $\bar{\Psi}^{(+)}$ is

$$\bar{\Psi}^{(+)}(\mathbf{X},\mathbf{Y}) = \frac{1}{2\pi i}\int d\mathbf{X'} d\mathbf{Y'} \int_{-\infty}^{\infty} dE_x G^{(+)}_{E_x}(\mathbf{X},\mathbf{X'}) \times G^{(+)}_{E_y}(\mathbf{Y},\mathbf{Y'}) \Delta V(X',Y') \Psi^{(+)}(\mathbf{X'Y'}).$$

The "initial" solution $\Psi^{(+)}$ of Eq. (19) rewritten in the coordinates X and Y is

$$\Psi^{(+)}_{JM}(\mathbf{X},\mathbf{Y}) = \frac{\varphi_{Ll_xl_yS}(X,Y)}{XY}[[l_y \otimes l_x]_L \otimes S]_{JM}. \quad (28)$$

The asymptotic form of the "corrected" continuum WF $\bar{\Psi}^{(+)}_{JM}$ is

$$\begin{aligned} \bar{\Psi}^{(+)}_{JM}(\mathbf{X},\mathbf{Y}) &= \frac{1}{2\pi i}\frac{E_{3r}}{XY}\int_0^1 d\varepsilon \frac{4}{v_x(\varepsilon)v_y(\varepsilon)} A(\varepsilon) \\ &\times e^{ik_x(\varepsilon)X + ik_y(\varepsilon)Y}[[l_y \otimes l_x]_L \otimes S]_{JM}, \\ E_x &= \varepsilon E_{3r}, \quad E_y = (1-\varepsilon)E_{3r}, \quad v_i(\varepsilon) = \sqrt{2E_i/M_i}, \\ A(\varepsilon) &= \int_0^R dX' \int_0^R dY' \varphi_{l_x}(k_x(\varepsilon)X')\varphi_{l_y}(k_y(\varepsilon)Y') \\ &\times \Delta V(X',Y')\varphi_{Ll_xl_yS}(X',Y'). \end{aligned} \quad (29)$$

The corrected outgoing flux j_c can be calculated on the sphere of the large radius for any of two Jacobi variables. For example, for the X coordinate, we have [4]

$$\begin{aligned} j_c(E_{3r}) &= {\rm Im}\left[X^2 \int d\Omega_x \int d\mathbf{Y} \left(\bar{\Psi}^{(+)*}\frac{\nabla_X}{M_x}\bar{\Psi}^{(+)}\right)\right]\Bigg|_{X\to\infty} \\ &= E^2_{3r}\int_0^1 d\varepsilon \frac{A^*(\varepsilon)}{2\pi}\frac{4}{v_x v_y}\int_0^1 d\varepsilon' \frac{k_x(\varepsilon)}{M_x}\frac{A(\varepsilon')}{2\pi} \\ &\times \frac{4}{v'_x v'_y} 2\pi\delta(k_y(\varepsilon') - k_y(\varepsilon)). \end{aligned} \quad (30)$$

Values v'_i above denote $v_i(\varepsilon')$. The flux is obtained as

$$j_c(E_{3r}) = \frac{8}{\pi}E_{3r}\int_0^1 d\varepsilon \frac{1}{v_x(\varepsilon)v_y(\varepsilon)}|A(\varepsilon)|^2. \quad (31)$$

[4]The derivation of the flux here is given in a schematic form. The complete proof is to bulky to be provided in the limited space. We mention only that it is easy to check directly that the derived expression for flux preserves the continuum normalization.

In principle, the widths obtained with both fluxes in Eqs. (18) and (31) should be equal, that is,

$$\Gamma = \frac{j}{N} \equiv \Gamma_c = \frac{j_c}{N}. \quad (32)$$

This is the idea of the calibration procedure for the simplified three-body model. The convergence of the HH method (for WF $\Psi^{(+)}_{JM}$) is *expected* to be fast in the internal region and much slower in the distant subbarrier region. This should affect the width Γ calculated in the HH method, which is sensitive to the asymptotic behavior of the WF. However, the procedure for calculation of the "corrected" width Γ_c is exact under the barrier, and it is sensitive only to HH convergence in the internal region, which is achieved easily. Below we demonstrate this in particular calculations.

IV. DECAYS OF THE ^{17}Ne $3/2^-$ AND ^{45}Fe $3/2^-$ STATES IN A SIMPLIFIED MODEL

In this section, when we refer to widths of ^{17}Ne and ^{45}Fe we always mean the ^{17}Ne $3/2^-$ state ($E_{3r} = 0.344$ MeV) and the ^{45}Fe $3/2^-$ ground state ($E_{3r} = 1.154$ MeV) calculated in very simple models. We expect that important regularities found for these models should be true also in realistic calculations. However, particular values obtained in realistic models may differ significantly, and this issue is considered specially in the Sec. V.

To keep only the most significant features of the systems, we assume a pure sd structure ($l_x = 0, l_y = 2$) for ^{17}Ne and a pure p^2 structure ($l_x = 1, l_y = 1$) for ^{45}Fe in the Y Jacobi system (see Fig. 2). Spin dependencies of the interactions are neglected. The Gaussian form factor

$$V^{\rm nuc}_i(r) = V_{i0}\exp[-(r/r_0)^2],$$

where $i = \{x, y\}$ is taken for ^{17}Ne (see Table I), and a standard Woods-Saxon form factor is used for ^{45}Fe (see Table II),

$$V^{\rm nuc}_i(r) = V_{i0}[1 + \exp[(r - r_0)/a]]^{-1}. \quad (33)$$

The simplistic structure models can be expected to overestimate the widths. There should be a considerable weight of d^2 component ($l_x = 2, l_y = 2$) in ^{17}Ne and f^2 component ($l_x = 3, l_y = 3$) in ^{45}Fe. Also, the spin-angular coupling should lead to splitting of the single-particle strength and corresponding reduction of the width estimates (e.g., we assume one s-wave state at 0.535 keV in the X subsystem of ^{17}Ne, while in reality there are two s-wave states in ^{16}F: 0^- at 0.535 MeV and 1^- at 0.728 MeV). Thus, the results of the simplified model should most likely be regarded as upper limits for widths.

A. One final state interaction: Core-p channel

First we take into account only the 0.535 MeV s-wave two-body resonance in the ^{16}F subsystem (this is the experimental energy of the first state in ^{16}F). Convergence of the ^{17}Ne width in a simplified model for the Y Jacobi system is shown in Fig. 3. The convergence of the corrected width Γ_c as a function of $K_{\rm max}$ is very fast: $K_{\rm max} > 8$ for the width is stable within $\sim$1%. For the maximal achieved in the fully dynamic

TABLE I. Parameters for ^{17}Ne calculations. Potential parameters for ^{15}O+p channel in s wave (V_{x0} in MeV, $r_0 = 3.53$ fm) and ^{16}F+p channel in d wave (V_{y0} in MeV). Radius of the charged sphere is $r_{\rm sph} = 3.904$ fm. Widths Γ_i of the state in the subsystem and experimental width values $\Gamma_{\rm exp}$ for really existing at these energies states are given in keV. The corrected three-body width Γ_c is given in the units 10^{-14} MeV. TFSI calculations with the d-wave state at 1.2 MeV are made with the s-wave state at 0.728 MeV.

E_{2r}	l_x (l_y)	V_{x0} (V_{y0})	Γ_x (Γ_y)	$\Gamma_{\rm exp}$	Γ_c
0.258	0	−14.4	0.221		144
0.275	0	−14.35	0.355		16.6
0.292	0	−14.3	0.544		7.75
0.360	0	−14.1	2.09		2.34
0.535	0	−13.55	17.9	25(5) [35]	0.545
0.728	0	−12.89	72.0	70(5) [35]	0.211
1.0	0	−12.0	252		0.093
2.0	0	−9.0	∼1500		0.021
0.96	2	−87.06	3.5	6(3) [35]	4.73[a]
1.256	2	−85.98	12.2	<15 [36]	2.0[a]
0.96	2	−66.46	3.6	6(3) [35]	1.37[b]
1.256	2	−65.4	13.7	<15 [36]	0.584[b]

[a]This is the TFSI calculation with "no p-p" Coulomb, $r_0 = 2.75$ fm.

[b]This is the TFSI calculation with "effective" Coulomb, $r_0 = 3.2$ fm.

calculation $K_{\rm max} = 24$, the three-body width Γ is calculated within 30% precision. Further increase of the effective basis size is possible within the adiabatic procedure based on the so-called Feschbach reduction (FR).

The Feschbach reduction is a procedure that eliminates from the total WF $\Psi = \Psi_p + \Psi_q$ an arbitrary subspace q using the Green's function of this subspace:

$$H_p = T_p + V_p + V_{pq} G_q V_{pq}.$$

In a certain adiabatic approximation, we can assume that the radial part of kinetic energy is small and constant under the centrifugal barrier (in the channels where the centrifugal barrier is much higher than any other interaction). In this approximation, the FR procedure becomes trivial, as it is reduced to the construction of effective three-body interactions

TABLE II. Parameters for ^{45}Fe calculations. Potential parameters for p-wave interactions [Eq. (33)] in ^{43}Cr+p channel (V_{x0} in MeV, $r_0 = 4.236$ fm, $r_{\rm sph} = 5.486$ fm) and ^{44}Mn+p (V_{y0} in MeV, $r_0 = 4.268$ fm, $r_{\rm sph} = 5.527$ fm), $a = 0.65$ fm. Calculations are made with the "effective Coulomb" of Eq. (22). Widths Γ_x, Γ_y of the states in the subsystems are given in keV. Corrected three-body widths are given in units of 10^{-19} MeV.

E_{2r}	V_{x0}	Γ_x	V_{y0}	Γ_y	Γ_c
1.0	−24.350	4.3×10^{-3}	−24.54	2.1×10^{-3}	23.4
1.2	−24.03	0.032	−24.224	0.018	10.4
1.48	−23.58	0.26	−23.78	0.15	4.94
2.0	−22.7	3.6	−22.93	2.3	2.02
3.0	−20.93	58	−21.19	44	0.74

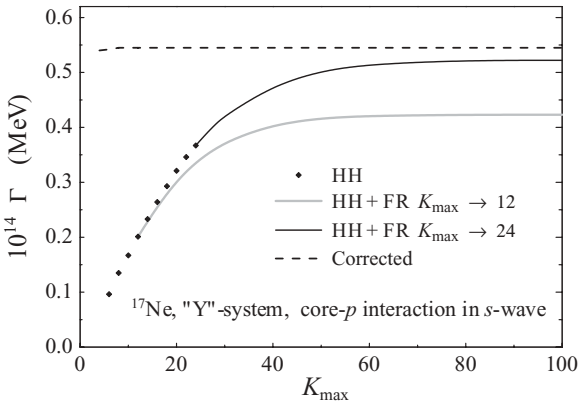

FIG. 3. Convergence of the ^{17}Ne width in a simplified model in the Y Jacobi system. OFSI model with experimental position $E_{2r} = 0.535$ KeV of the s-wave two-body resonance. Diamonds show the results of dynamic HH calculations. Solid curves correspond to calculations with effective FR potentials.

$V^{\rm eff}_{K\gamma,K'\gamma'}$ by matrix operations

$$G^{-1}_{K\gamma,K'\gamma'} = (H-E)_{K\gamma,K'\gamma'} = V_{K\gamma,K'\gamma'} + \left[E_f - E + \frac{(K+3/2)(K+5/2)}{2M\rho^2}\right]\delta_{K\gamma,K'\gamma'},$$

$$V^{\rm eff}_{K\gamma,K'\gamma'} = V_{K\gamma,K'\gamma'} + \sum V_{K\gamma,\bar{K}\bar{\gamma}} G_{\bar{K}\bar{\gamma},\bar{K}'\bar{\gamma}'} V_{\bar{K}'\bar{\gamma}',K'\gamma'}.$$

Summation over indexes with bar is made for eliminated channels. No strong sensitivity to the exact value of the "Feshbach energy" E_f is found, and we take it as $E_f \equiv E$ in our calculations. More detailed account of the procedure applied within HH method can be found in Ref. [37].

It can be seen in Fig. 3 (solid line) that the Feschbach reduction procedure drastically improves the convergence. However, the calculation converges to a width value, which is somewhat smaller than the corrected width value (that should be exact). The reason for this effect can be understood if we make a reduction to a smaller "dynamic" basis size ($K_{\rm max} = 12$, gray line). The calculation in these conditions also converges, but even to a smaller width value. We can conclude that the FR procedure allows us in any case to approach the real width value from below, but it provides a precise result only for sufficiently large size of the dynamic sector of the basis.

The next issue to be discussed is a convergence of the width in calculations with different positions E_{2r} of the two-body resonance in the core+p subsystem. It is demonstrated for several energies E_{2r} in Fig. 4. When the resonance in the subsystem is absent (or located relatively high), the convergence of the width value to the exact result is very fast both in the pure three-body and in the corrected calculation (in that case, however, much faster). Here even FR is not required, as the convergent result is achieved in the HH calculations by $K_{\rm max} = 10$–24. The closer the two-body resonance approaches the decay window, the worse is the convergence of the HH calculations. At energy $E_{2r} = 360$ keV (which is already close

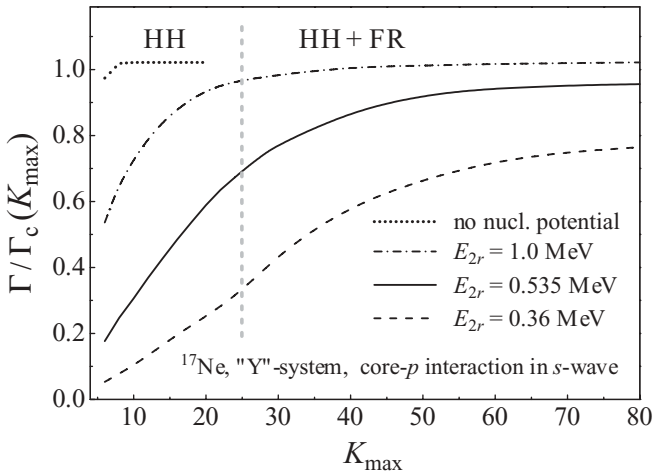

FIG. 4. Convergence of widths in OFSI model for different positions E_{2r} of the two-body resonance in the core-p channel (Y Jacobi system). For $K_{max} > 24$, the value of K_{max} denotes the size of the basis for the Feshbach reduction to $K_{max} = 24$.

to the three-body decay window $E_{3r} = 344$ keV) even the FR procedure provides a convergence to the width value which is only about 65% of the exact value.

In Fig. 5, the calculations with different E_{2r} values are summarized. The width grows rapidly as the two-body resonance moves closer to the decay window. The penetrability enhancement provided by the two-body resonance even before it moves into the three-body decay window is very important. Difference of widths with no core-p FSI and FSI providing the s-wave resonance to be at its experimental position $E_{2r} = 0.535$ MeV is more than two orders of magnitude.

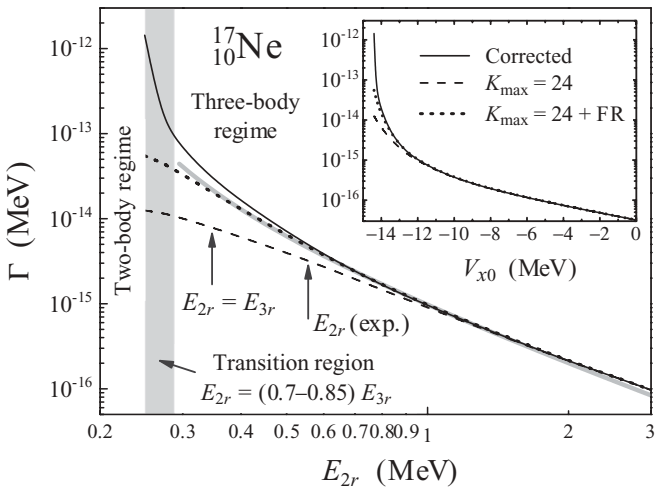

FIG. 5. Width of the ^{17}Ne $3/2^-$ state as a function of two-body resonance position E_{2r}. Dashed, dotted, and solid lines show cases of pure HH calculations with $K_{max} = 24$, the same but with Feshbach reduction from $K_{max} = 100$, and the corrected width Γ_c. Inset shows the same, but as a function of the potential depth parameter V_{x0}. Gray area shows the transition region from the three-body to the two-body decay regime. The gray curve shows the simple analytical dependence of Eq. (34).

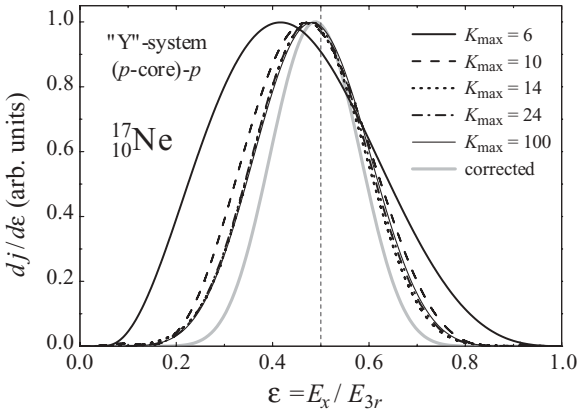

FIG. 6. Convergence of energy distribution for ^{17}Ne in the Y Jacobi system.

The convergence of HH calculations also deteriorates as E_{2r} moves closer to the decay window. However, the disagreement between the HH width and the exact value is within an order of magnitude, until the resonance achieves the range $E_{2r} \sim (0.7–0.85)E_{3r}$. Within this range, a transition from the three-body to the two-body regime happens (see also discussion in Ref. [8]), which can be seen as a drastic change of the width dependence on E_{2r}. This means that a sequential decay via two-body resonance E_{2r} becomes more efficient than the three-body decay. In that case, the hyperspherical expansion cannot treat the dynamics efficiently any more, and the disagreement with an exact result becomes as large as orders of magnitude. The decay dynamics in the transition region is also discussed in details below.

It can be seen in Fig. 5 that in the three-body regime, the dependence of the three-body width follows well the analytical expression

$$\Gamma \sim (E_{3r}/2 - E_{2r})^{-2}. \tag{34}$$

The reasons for such a behavior will be clarified in the companion paper [22]. The deviations from this dependence can be found in the decay window (close to the "transition regime") and at higher energies. This dependence is quite universal; e.g., for ^{45}Fe it is demonstrated in Fig. 14, where it follows the calculation results even with higher precision.

Another important issue is a convergence of energy distributions in the HH calculations, demonstrated in Fig. 6 for calculations with $E_{2r} = 535$ keV. The distribution is calculated in the Y Jacobi system; thus E_x is the energy between the core and one proton. The energy distribution convergence is fast: the distribution is stable at $K_{max} = 10$–14 and does not change visibly with a further increase of the basis. There remains a visible disagreement with the exact (corrected) results, which give a narrower energy distribution. We think that this effect was understood in our work [4]. The three-body calculations are typically done for $\rho_{max} \sim 500$–2000 fm ($\rho_{max} = 1000$ fm everywhere in this work). It was demonstrated in Ref. [4] by construction of classical trajectories that we should expect a complete stabilization of the energy distribution in the core+p

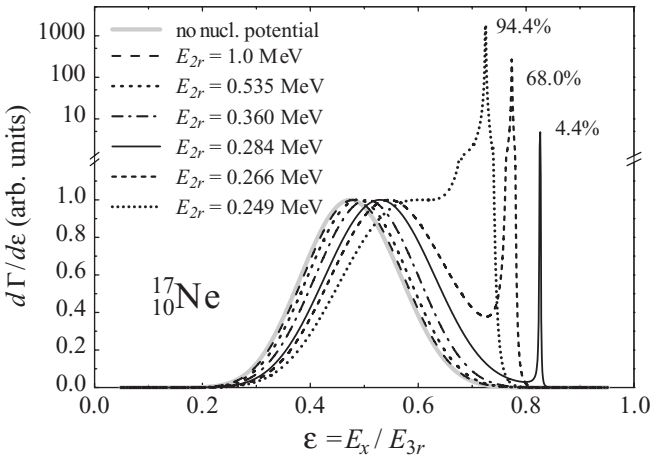

FIG. 7. Energy distributions for ^{17}Ne in the Y Jacobi system for different two-body resonance positions E_{2r}. The three-body decay energy is $E_{3r} = 0.344$ MeV. The distributions are normalized to have unity value on a maximum of three-body components. The values near the peaks show the fraction of the total intensity concentrated within the peak. Note the change of the scale on the vertical axis.

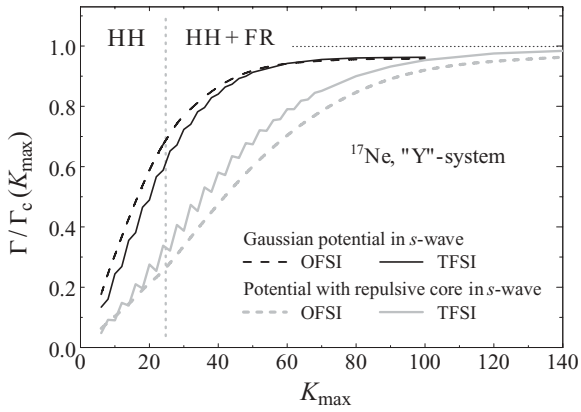

FIG. 8. Convergence of the ^{17}Ne width in a simplified model, Y Jacobi system. OFSI model with s-wave two-body resonance at $E_{2r} = 0.535$ MeV; Gaussian potential and potential with repulsive core. TFSI model with d-wave two-body resonance at $E_{2r} = 0.96$ MeV.

subsystem at $\rho_{max} \sim 30\,000$–$50\,000$ fm, and the effect on the width of the energy distribution should be comparable to the one observed in Fig. 6.

The evolution of the energy distribution in the core+p subsystem with variation of E_{2r} is shown in Fig. 7. When we decrease the energy E_{2r} the distribution is very stable until the two-body resonance enters the three-body decay energy window. After that, first the peak at about $\varepsilon \sim 0.5$ drifts to a higher energy, and then for $E_{2r} \sim 0.85E_{3r}$ the noticeable second narrow peak for sequential decay is formed. At $E_{2r} \sim 0.7E_{3r}$ the sequential peak becomes so high that the three-body component of the spectrum practically disappears in the background.

The result concerning the transition region obtained in this model is consistent with the conclusion of Ref. [8] (where a much simpler model was used for making estimates). Three-body decay is the dominant decay mode not only when the sequential decay is energy prohibited as $E_{2r} > E_{3r}$, but also when the sequential decay is formally allowed (because $E_{2r} < E_{3r}$) but does not take place in reality because of Coulomb suppression at $E_{2r} \gtrsim 0.8E_{3r}$.

Geometric characters of potentials can play an important role in the width convergence. To test this aspect of the convergence, we have also made calculations for the potential with a repulsive core. This class of potentials was employed in studies of ^{17}Ne and ^{19}Mg in Ref. [7]. A comparison of the convergence of HH calculations with s-wave ^{15}O+p potential from Ref. [7] and Gaussian potential is given in Fig. 8. The width convergence in the case of the "complicated" potential with a repulsive core is drastically worse than in the "easy" case of Gaussian potential. For typical dynamic calculations with $K_{max} = 20$–24, the HH calculations provide only 20–25% of the width for the potential with a repulsive core. On the other hand, the calculations with both potentials provide practically the same widths Γ_c,[5] and FR provides practically the same and very well converged results in both cases.

B. One final state interaction: p-p channel

Because two-proton decay is often interpreted as "diproton" decay, we should also consider this case and study how important this channel could be. For this calculation, we use a simple s-wave Gaussian p-p potential, providing a good low-energy p-p phase shift,

$$V(r) = -31 \exp\left[-(r/1.8)^2\right]. \tag{35}$$

Calculations with this potential are shown in Fig. 9 (see also Table V). First of all, the penetrability enhancement provided by the p-p FSI is much less than the enhancement provided

[5]We demonstrate in paper [22] that a three-body width should depend linearly on two-body widths of the subsystems and only very weakly on various geometrical factors. This is confirmed very well by direct calculations.

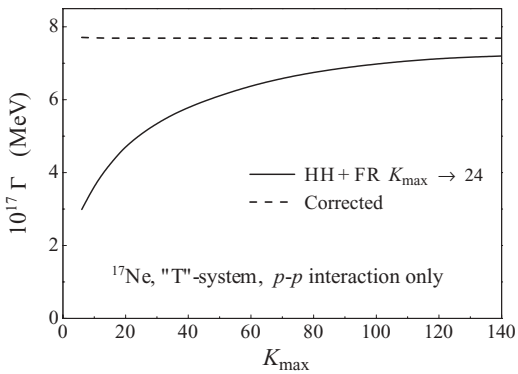

FIG. 9. Convergence of the ^{17}Ne width in a simplified model, T Jacobi system. Final state interaction describes s-wave p-p scattering.

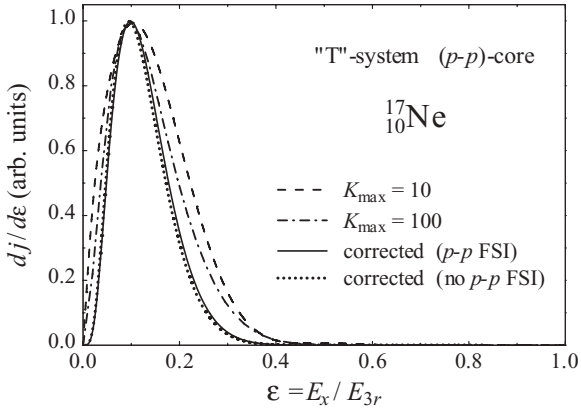

FIG. 10. Energy distributions for ^{17}Ne in the T Jacobi system (between two protons).

by the core-p FSI (widths differ by more than two orders of magnitude, see Fig. 3). This is the feature that has already been outlined in our previous works. The p-p interaction may strongly boost the penetrability, but only in the situation when protons occupy predominantly orbitals with high orbital momenta. In such a situation, the p-p interaction allows transitions to configurations with smaller orbital momenta in the subbarrier region, which provide a large increase of the penetrability. In our simple model for the ^{17}Ne $3/2^-$ state, we have already assumed the population of orbitals with minimal possible angular momenta, and thus no strong effect of the p-p interaction is expected.

Also, a very slow convergence of the decay width should be noted in this case. For the core-p interaction, $K_{\max} \sim 10$–40 is sufficient to obtain a reasonable result. In the case of the p-p interaction, $K_{\max} \sim 100$ is required.

Energy distributions between two protons obtained in this model are shown in Fig. 10. An important feature of these distributions is a strong focusing of protons at small p-p energies. This feature is connected, however, not with an attractive p-p FSI, but with a dominating Coulomb repulsion in the core-p channel. This is demonstrated by the calculation with nuclear FSI turned off, which provides practically the same energy distributions. Similar to the case of the core-p FSI, very small $K_{\max} \gtrsim 10$ is sufficient to provide the well-converged energy distribution. The converged HH distribution is very close to the exact (corrected) one, but it is, again, somewhat broader.

So far the diproton model has been treated by us as a reliable upper limit for the three-body width [8]. With some technical improvements, this model was used for the two-proton widths calculations in Refs. [16–19]. It is important therefore to try to understand qualitatively the reason for the small width values obtained in this form of the OFSI model, which evidently represents *an appropriately formulated diproton model*.[6] In Fig. 11, we compare the results of the OFSI calculations for

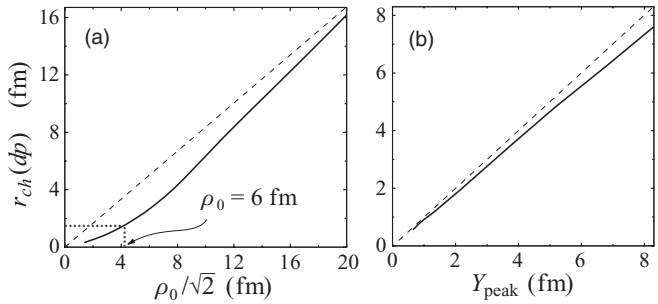

FIG. 11. Comparison of the OFSI calculations for ^{45}Fe in the T system with diproton model Eq. (36). Solid lines show effective equivalent channel radius $r_{\rm ch}(dp)$ for "diproton emission" as a function of (a) radius ρ_0 of the three-body potential [Eq. (25)], where the value $\rho_0/\sqrt{2}$ should be comparable with typical nuclear sizes, and (b) position of the peak $Y_{\rm peak}$ in the three-body WF $\Psi^{(+)}$ in the Y coordinate. The dashed lines are given to guide the eye.

^{45}Fe in the T system with the diproton width estimated by the expression

$$\Gamma_{dp} = \frac{1}{M_{\rm red} r_{\rm ch}^2(dp)} P_{l=0}(0.95E_{3r}, r_{\rm ch}(dp), 2Z_{\rm core}), \qquad (36)$$

where $M_{\rm red}$ is the reduced mass for ^{43}Cr-pp motion, and $r_{\rm ch}(dp)$ is the channel radius for diproton emission. The energy for the relative ^{43}Cr-pp motion is taken to be $0.95E_{3r}$ based on the energy distribution in the p-p channel (see Fig. 10, for example). In Fig. 11(a), we show the effective equivalent channel radii for diproton emission obtained by fulfilling condition $\Gamma_{dp} \equiv \Gamma_c$ for OFSI model calculations with different radii ρ_0 of the three-body potential Eq. (25). It is easy to see that for realistic values of these radii ($\rho_0 \sim 6$ fm for ^{45}Fe), the equivalent diproton model radii should be very small ($\sim$1.5 fm). This happens presumably because the diproton is too large to be considered as emitted from the nuclear surface of such a small ρ_0 radius. Technically it can be seen as the nonlinearity of the $r_{\rm ch}(dp)$-ρ_0 dependence, with the linear region achieved at $\rho_0 \sim 15$–20 fm. A^+ such unrealistically large ρ_0 values the nuclear surface radius becomes comparable with the "size" of the diproton. Only in these conditions the nuclear surface can be reasonably interpreted as the surface of the diproton emission. It is interesting to note that in the nonlinearity region for Fig. 11(a) there exists practically exact linear correspondence between the Y coordinate of the WF peak in the internal region and the channel radius for diproton emission [Fig. 11(b)]. This fact is reasonable to interpret in such a way that the diproton is actually emitted not from the nuclear surface (as presumed by the existing systematics of diproton calculations) but from the interior region, where the WF is mostly concentrated.

C. Two final state interactions

As we have already mentioned, the situation of one final state interaction is convenient for studies but rarely realized in practice. An exception is the case of the $E1$ transitions to continuum in the three-body systems, considered in our

[6]The assumed nuclear structure is very simple, but the diproton penetration process is treated exactly, without assumptions about the emission of the diproton from some nuclear surface, which should be made in the R-matrix approach.

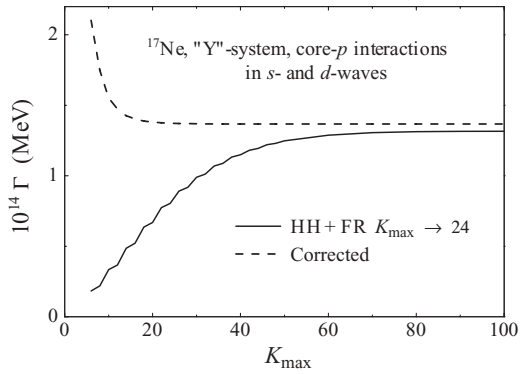

FIG. 12. Convergence of the ^{17}Ne width for experimental positions $E_{2r} = 0.535$ MeV of the 0^+ two-body resonance in the X subsystem and $E_{2r} = 0.96$ MeV of the 2^+ two-body resonance in the Y subsystem (TFSI model).

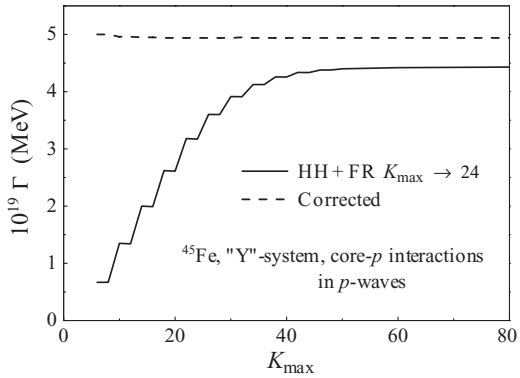

FIG. 13. Convergence of the ^{45}Fe width for position of the 1^- two-body resonances in X and Y subsystems $E_{2r} = 1.48$ MeV.

previous work [24]. For narrow states in a typical nuclear system of the interest, there are at least two comparable final state interactions (in the core-p channel). For systems with heavy core, this situation can be treated reasonably well, because the Y coordinate (in the Y Jacobi system) for such systems practically coincides with the core-p coordinate. Below we treat in this way ^{17}Ne (for which this approximation could be not very consistent) and ^{45}Fe (for which this approximation should be good). In the case of ^{17}Ne, we are thus interested in the scale of the effect, rather than in the precise width value.

For calculations with two FSI for ^{17}Ne, we used the Gaussian d-wave potential (see Table I), in addition to the s-wave potential used in Sec. IV A. This potential provides a d-wave state at 0.96 MeV ($\Gamma = 13.5$ keV), which corresponds to the experimental position of the first d-wave state in ^{16}F. The convergence of the ^{17}Ne decay width is shown in Fig. 12. Comparing it with Fig. 3, one can see that the absolute value of the width has changed significantly (two to three times) but not extremely, and the convergence is practically the same. An interesting new feature is a kind of convergence curve "staggering" for odd and even values of $K/2$. Also, the convergence of the corrected calculations requires now a considerable $K_{max} \sim 12$–14.

The improved experimental data for the $2p$ decay of ^{45}Fe was published recently in Ref. [12]: $E_{3r} = 1.154(16)$ MeV, $\Gamma_{2p} = (1.62 \pm 0.38) \times 10^{-19}$ MeV [$T_{1/2} = 1.6^{+0.5}_{-0.3}$ ms with two-proton branching ratio Br$(2p) = 0.57$]. In this paper we use the resonance energy from this work.

The convergence of the ^{45}Fe width is shown in Fig. 13. The character of this convergence is very similar to that in the ^{17}Ne case, except the staggering feature is more expressed.

The dependence of the ^{45}Fe width on the two-body resonance energy E_{2r} is shown in Fig. 14. Potential parameters for these ^{45}Fe calculations are given in Table II. The result calculated for $E_{3r} = 1.154$ MeV and $E_{2r} = 1.48$ MeV in paper [4] for pure $[p^2]$ configuration is $\Gamma = 2.85 \times 10^{-19}$ MeV. The value $K_{max} = 20$ was used in these calculations. If we take the HH width value from Fig. 13 at $K_{max} = 20$, it provides $\Gamma = 2.62 \times 10^{-19}$ MeV, which is in good agreement with a full HH three-body model of Ref. [4]. However, from Fig. 13, we can conclude that the calculations of Ref. [4] underestimated the width by about 47%. Thus the value of about $\Gamma = 5.6 \times 10^{-19}$ MeV should be expected in these calculations. On the other hand, much larger uncertainty could be inferred from Fig. 14 because of the uncertain energy of the ^{44}Mn ground state. If we assume a variation $E_{2r} = 1.1$–1.6 MeV, the inferred from Fig. 14 uncertainty of the width would be $\Gamma = (4$–$16) \times 10^{-19}$ MeV. On top of that, we expect a strong p^2/f^2 configuration mixing which could easily reduce the width within an order of magnitude. Thus we can conclude that better knowledge of the spectrum of ^{44}Mn and reliable structure information about ^{45}Fe are still required to make sufficiently precise calculations of the ^{45}Fe width. A more detailed account of these issues is provided below.

V. THREE-BODY CALCULATIONS

Having in mind the experience of the convergence studies, we next perform large-basis calculations for ^{45}Fe and ^{17}Ne. They are made with dynamical $K_{max} = 16$–18 (including

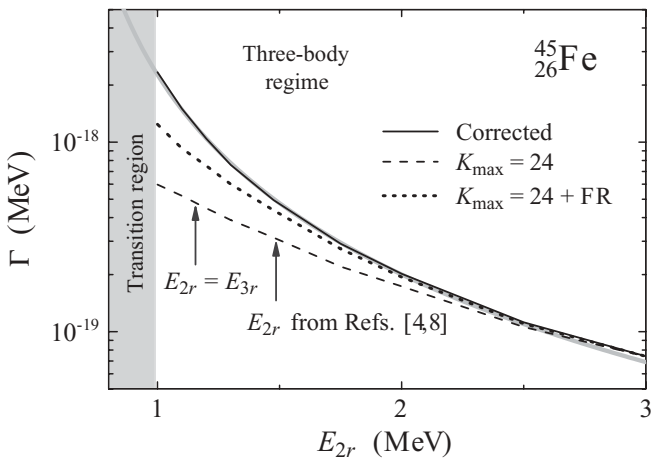

FIG. 14. ^{45}Fe g.s. width as a function of E_{2r}. Dashed, dotted, and solid lines show, respectively, a pure HH calculation with $K_{max} = 24$, the same but with Feshbach reduction from $K_{max} = 100$, and the corrected width Γ_c. Gray area shows the transition region from three-body to two-body decay regime. Gray curve shows simple analytical dependence of Eq. (34).

TABLE III. Low-lying states of ^{16}F obtained in the GMZ and high-s core-p potentials. The potentials are diagonal in the representation with definite total spin of core and proton S, which is given in the third column.

Case			GMZ		High-s		Exp.
J^π	l	S	E_{2r} (MeV)	Γ (keV)	E_{2r} (MeV)	Γ (keV)	Γ (keV)
0^-	0	0	0.535	18.8	0.535	18.8	25(5) [35]
1^-	0	1	0.728	73.4	0.728	73.4	70(5) [35]
2^-	2	0	0.96	3.5	0.96	3.5	6(3) [35]
3^-	2	1	1.2	9.9	1.2	10.5	<15 [36]
2^-	2	1	3.2	430	7.6	∼3000	
1^-	2	1	4.6	1350	∼15	∼6000	

Fechbach reduction from $K_{\max} = 30 - 40$) for ^{17}Ne and $K_{\max} = 20$ (FR from $K_{\max} = 40$) for ^{45}Fe. The calculated width values are extrapolated using the convergence curves obtained in the TFSI model (Fig. 15 for ^{17}Ne and Fig. 13 for ^{45}Fe). We have no proof that the width convergence in the realistic three-body case is absolutely the same as in the TFSI case. However, the TFSI model takes into account the main dynamic features of the system causing a slow convergence, and we are expecting that the convergence should be nearly the same in both cases.

A. Widths and correlations in ^{17}Ne

The potentials used in the realistic calculations are the same as those used for ^{17}Ne studies in Refs. [7,38]. The realistic nucleon-nucleon potential [39] is used in the p-p channel. The core-p potentials are referred to in Ref. [38] as "GMZ" (potential introduced in Ref. [7]) and "high s" (with centroid of d-wave states shifted upward which provides a higher content of s^2 components in the ^{17}Ne g.s. WF). Both potentials provide correct low-lying spectrum of ^{16}F and differ only for the d-wave continuum above 3 MeV (see Table III). The core-p nuclear potentials, including central, ss, and ls terms, are taken as

$$V(r) = \frac{V_c^l + (\mathbf{s}_1 \cdot \mathbf{s}_2)V_{ss}^l}{1 + \exp\left[(r - r_0^l)/a\right]} - (\mathbf{l} \cdot \mathbf{s})\frac{2.0153 V_{ls}^l}{ar} \times \exp\left[(r - r_0^l)/a\right]\left(1 + \exp\left[(r - r_0^l)/a\right]\right)^{-2}, \quad (37)$$

where $\mathbf{s} = \mathbf{s}_1 + \mathbf{s}_2$. The parameters are $a = 0.65$ fm, $r_0^0 = 3.014$ fm, $r_0^{l>0} = 2.94$ fm, $V_c^0 = -26.381$ MeV, $V_c^1 = -9$ MeV, $V_c^2 = -57.6(-51.48)$ MeV, $V_c^3 = -9$ MeV, $V_{ss}^0 = 0.885$ MeV, $V_{ss}^2 = 4.5(12.66)$ MeV, $V_{ls} = 4.4(13.5)$ MeV (the values in brackets are for the "high s" case). There are also repulsive cores for s and p waves described by $a = 0.4$ fm, $r_0^0 = 0.89$ fm, and $V_{\text{core}} = 200$ MeV. These potentials are used together with the Coulomb potential obtained for Gaussian charge distribution reproducing the charge radius of ^{15}O.

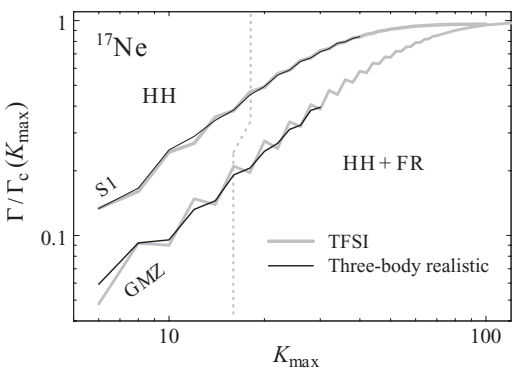

FIG. 15. Interpolation of ^{17}Ne decay width obtained in full three-body calculations by means of TFSI convergence curves (see Fig. 8). Upper curves correspond to the TFSI case with Gaussian potential in the s-wave and compatible S1 case for the full three-body model. Lower curves correspond to the TFSI case with repulsive core potential in the s-wave and compatible GMZ case for the full three-body model.

To have extra confidence in the results, the width of the ^{17}Ne $3/2^-$ state is calculated in several models of growing complexity (Tables IV–VI). One can see from these tables that improvements introduced on each step provide quite a smooth transition from the very simple to the most sophisticated model.

In Table IV, we demonstrate how the calculations in the simplified model of Sec. IV compare with calculations of the full three-body model with an appropriately truncated Hamiltonian. We can switch off corresponding interactions in the full model to make it consistent with the approximations of the simplified model. Remember, the differences between the full and simplified models are the following: (i) antisymmetrization between protons is missing, (ii) the Y coordinate is only approximately equal to the coordinate between the core and second proton, and (iii) the Coulomb interaction between protons (in the Y system) can be treated only effectively in the simplified model. Despite these approximations, the models demonstrate quite close results: the worst disagreement is a factor of 3, and in simplistic cases much better agreement is obtained.

In Table V we compare approximations of a different kind: those connected with the choice of the Jacobi coordinate system in the simplified model. First we compare the pure Coulomb case: all pairwise nuclear interactions are off and the existence of the resonance is provided solely by the three-body potential (25). This model provides some hint of what should be the width of the system without nuclear pairwise interactions. Then the models are compared with the

TABLE IV. Comparison of widths for ^{17}Ne (in 10^{-14} MeV units) obtained in simplified model in Y Jacobi system and in full three-body model with correspondingly truncated Hamiltonian. Structure information is provided for the three-body model. In the simplified model, the weight of the [sd] configuration is 100% by construction. The "no p-p" column shows the case where Coulomb interaction in the p-p channel is switched off [see Eq. (21) for simplified model]. "Eff." column corresponds to the effective treatment [see Eq. (22)] of the Coulomb interaction in the p-p channel in the simplified model, but to the exact treatment in the full three-body model.

	Pure Coulomb		OFSI		TFSI	
	No p-p	Eff.	No p-p	Eff.	No p-p	Eff.
Simpl.	0.017	0.0032	3.02	0.545	4.70	1.37
3-body	0.024[a]	0.0041[a]	3.22	0.555	3.91	0.445
[sd]	99.8	99.3	99.6	99.5	92.0	72.6
[p^2]	0.2	0.6	0.3	0.4	0.1	0.2
[d^2]	0	0	0	0	7.8	27.1

[a]Small repulsion (∼0.5 MeV) was added in that case in the p-wave core-p channel to split the states with sd and p^2 structure which appear practically degenerated and strongly mixed in this model.

nuclear FSIs added. The addition of nuclear FSIs drastically increases width in all cases. It is the most efficient (in the sense of width increase) in the case of the TFSI model in the Y system. Choice of this model provides the largest widths and can be used for the upper limit estimates.

In Table VI the full three-body models are compared. The simplistic S1 and S2 interactions correspond to calculations with simplified spectra of the ^{16}F subsystem. For the S1 case, it includes one s-wave state at 0.535 MeV ($\Gamma = 18.8$ keV) and one d-wave state at 0.96 MeV ($\Gamma = 3.5$ keV). These are two lower s- and d-wave states known experimentally. In the S2 case, we use instead the experimental positions of the higher component of the s- and d-wave doublets: s wave at 0.72 MeV ($\Gamma = 73.4$ keV) and d wave at 1.2 MeV ($\Gamma = 10$ keV). Parameters of the core-p potentials can be found in Table I. The simple Gaussian p-p potential [Eq. (35)] is used. The variation of the results between these models is moderate (∼30%). The calculations with the GMZ potential provide the width for the ^{17}Ne $3/2^-$ state which comfortably rests in between the results obtained in the simplified S1 and S2 models. The structure of the WF is also obtained quite close to these calculations. The structure in the high-s case is obtained with a strong domination of the sd component. The width obtained in the high-s case is somewhat larger (∼11%) than obtained in GMZ case, but this increase is consistent with the increase of the sd WF component (∼15%), which is expected to be more preferable for decay than d^2 component.

It is important for us that the results obtained in the three-body models with considerably varying spectra of the two-body subsystems and different convergence systematics appear to be quite close: $\Gamma \sim (5\text{–}8) \times 10^{-15}$ MeV. Thus we have not found a factor which could lead to a considerable variation of the three-body width, given the ingredients of the model are reasonably realistic.

The decomposition of the ^{17}Ne WF obtained with GMZ potential is provided in Table VII in terms of partial internal normalizations $N^{(i)}_{K\gamma}$ (in the T and Y Jacobi systems, $i = \{T, Y\}$) and partial widths. The correspondence between the components with large weights and large partial widths is typically good. However, there are several components giving large contributions to the width in spite of their negligible presence in the interior.

Complete correlation information for three-body decay of a resonant state (with omission of spin degrees of freedom) can be described by two variables. We use the energy distribution

TABLE V. Comparison of widths calculated for ^{17}Ne (10^{-14} MeV units) and ^{45}Fe (10^{-19} MeV units) with pure Coulomb FSIs and for nuclear plus Coulomb FSIs. Simplified OFSI model in T, TFSI in Y Jacobi systems ("effective" Coulomb is used in both cases) and full three-body calculations (denoted "3-body").

	Pure Coulomb			Nuclear + Coulomb		
	T	Y	3-body	T	Y	3-body
^{17}Ne	0.0011	0.0032	0.0041	0.0077	1.37	0.76[a]
[sd]	100	100	99.3	100	100	73.1
[p^2]	0	0	0.6	0	0	1.8
[d^2]	0	0	0	0	0	24.2
^{45}Fe	0.0053	0.0167	0.26	0.034	4.94	6.3[b]

[a]Calculation with S1 Hamiltonian.
[b]Calculation providing pure p^2 structure.

TABLE VI. Width (in 10^{-14} MeV units) and structure of ^{17}Ne $3/2^-$ state calculated in a full three-body model with different three-body Hamiltonians.

	S1	S2	GMZ	High-s
$K_{\max} = 18$	0.35	0.27	0.14	0.16
Extrapolated	0.76	0.56	0.69	0.76
[sd]	73.1	71.7	80.2	95.1
[p^2]	1.8	1.8	2.0	1.3
[d^2]	24.2	25.7	16.8	3.1

TABLE VII. Partial widths $\Gamma_{K\gamma}$ of different components of ^{17}Ne $3/2^-$ WF calculated in T Jacobi system. Partial weights are given in Y, $N^{(Y)}_{K\gamma}$, and in T, $N^{(T)}_{K\gamma}$, Jacobi systems. S_x is the total spin of two protons. All listed components have total spin of core and protons $S = 1/2$.

K	L	l_x	l_y	S_x	$N^{(Y)}_{K\gamma}$	$N^{(T)}_{K\gamma}$	$\Gamma_{K\gamma}$
2	2	0	2	0	23.88	33.87	44.93
2	2	2	0	0	24.97	16.52	13.29
2	2	1	1	1	0.28	7.39	3.59
2	2	1	1	0	1.54		
2	2	0	2	1	3.68		
2	2	2	0	1	3.68		
4	2	0	2	0	8.97	20.04	3.19
4	2	2	0	0	8.68	13.57	5.57
4	2	2	2	0	15.49	0.32	18.80
4	2	1	3	1	0.03	2.18	0.95
4	2	3	1	1	0	1.89	0.63
4	1	2	2	1	1.02		
4	2	0	2	1	1.99		
4	2	2	0	1	2.07		
6	2	2	4	0	0.14	0.77	3.57
6	2	4	2	0	0.14	0.77	0.78
6	2	0	2	0	0.50	0.09	0.69
8	2	4	4	0	0.02	0.003	1.58

parameter $\varepsilon = E_x/E_{3r}$ and the angle $\cos(\theta_k) = (\mathbf{k}_x\mathbf{k}_y)/(k_x k_y)$ between the Jacobi momenta (see Ref. [4] for details). The complete correlation information is provided in Fig. 16 for realistic ^{17}Ne $3/2^-$ decay calculations. We can see that the profile of the energy distribution is characterized by formation of the double-hump structure, expected so far for the p^2 configurations (see, e.g., Ref. [4]). This structure can be seen in both the T system (in energy distribution) and the Y system (in angular distribution). In the calculations of ground states of the sd shell nuclei, we were getting such distributions to be quite smooth. It can be found that for the excited state the profile of this distribution is defined by the sd/d^2 components ratio. For example, in the calculations with high-s potential, the total domination of the sd configuration leads to washing out of the double-hump profile.

The correlations in the ^{17}Ne (shown in Fig. 16) are strongly influenced by the nuclear FSIs. Calculations for only Coulomb pairwise FSIs left in the Hamiltonian are shown in Fig. 17. The strong peak at small p-p energy is largely dissolved, and the most prominent feature of the correlation density in that case is a rise of the distribution for $\cos(\theta_k) \to 1$ in the Y Jacobi system. This kinematical region corresponds to the motion of protons in the opposite direction relative to the core and is a qualitatively understandable feature of the three-body Coulomb interaction (the p-p Coulomb interaction is minimal along such a trajectory).

The distributions calculated in the simplified (OFSI) model are shown in Fig. 18 on the same $\{\varepsilon, \cos(\theta_k)\}$ plane as in Figs. 16 and 17. Note that in Fig. 18 the calculations in the T and Y Jacobi systems represent different calculations (with p-p FSI only and with core-p FSI only). In contrast, in Figs. 16 and 17 two panels show different representations of the same

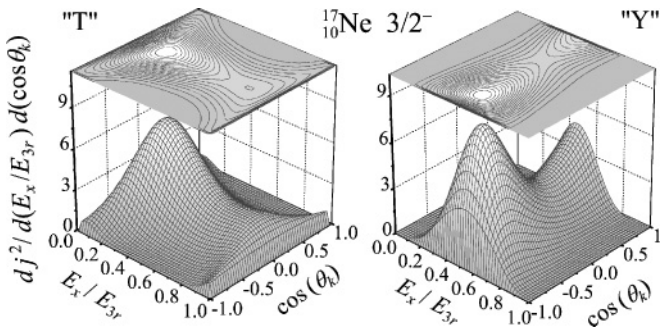

FIG. 16. Correlations for ^{17}Ne decay in T and Y Jacobi systems. Three-body calculations with realistic (GMZ) potential.

result. Providing reasonable (within factor 2–4) approximation to the full three-body model in the sense of the decay width, the simplified model is very deficient in the sense of correlations. The only feature of the realistic correlations which is even qualitatively correctly described in the simplified model is the energy distribution in the Y system. The diproton model (OFSI model with p-p interaction) fails especially strongly, which is certainly relevant to the very small width provided by this model (see discussion in the Sec. IV B).

B. Width of ^{45}Fe

The calculation strategy is the same as in Ref. [4]. We start with interactions in the core-p channel which give a resonance in the p-wave at fixed energy E_{2r}. Such a calculation provides ^{45}Fe with a practically pure p^2 structure. Then we gradually increase the interaction in the f wave until it replaces the p-wave resonance at fixed E_{2r} and then we gradually move the p-wave resonance to high energy. Thus we generate a set of WFs with different p^2/f^2 mixing ratios.

The results of the improved calculations with the same settings as in Ref. [4] (the ^{44}Mn g.s. is fixed to have $E_{2r} = 1.48$ MeV) are shown in Fig. 19 (see also Table V) together with available experimental data [9,10,12]. The basis size used in Ref. [4] was sufficient to provide stable correlation pictures (as we have found in this work), and they are not updated.

The sensitivity of the obtained results to the experimentally unknown energy of ^{44}Mn can be easily studied by means of Eq. (34). The results are shown in Fig. 20 in terms of the regions

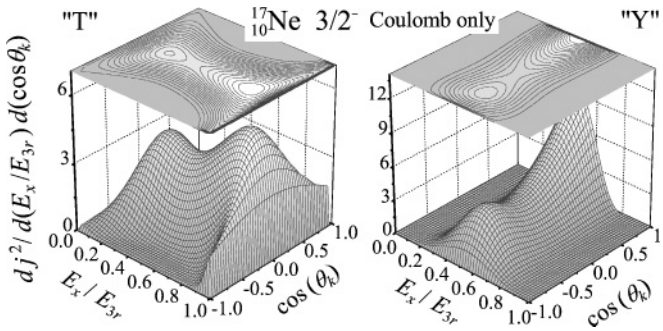

FIG. 17. Correlations for ^{17}Ne decay in T and Y Jacobi systems. Three-body calculations with Coulomb FSIs only (all nuclear pairwise potentials are turned off).

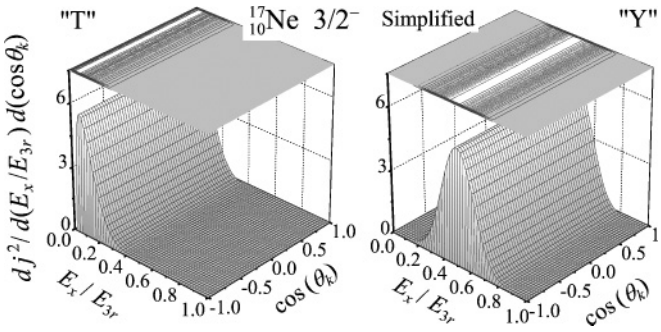

FIG. 18. Correlations for ^{17}Ne decay calculated in simplified OFSI model in T (only p-p FSI) and Y Jacobi systems (only s-wave core-p FSI).

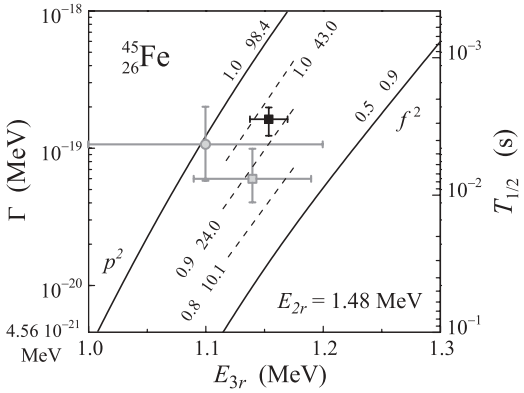

FIG. 19. Lifetime of ^{45}Fe as a function of the $2p$ decay energy E_{3r}. The plot is the analog of Fig. 6(a) from Ref. [4] with experimental data [9] (gray circle), [10] (gray rectangle), [12] (black rectangle), and improved theoretical results. Solid curves show the cases of practically pure p^2 and f^2 configurations, dashed curves stand for different mixed p^2/f^2 cases. The numerical labels on the curves show the weights of the s^2 and p^2 configurations in percents.

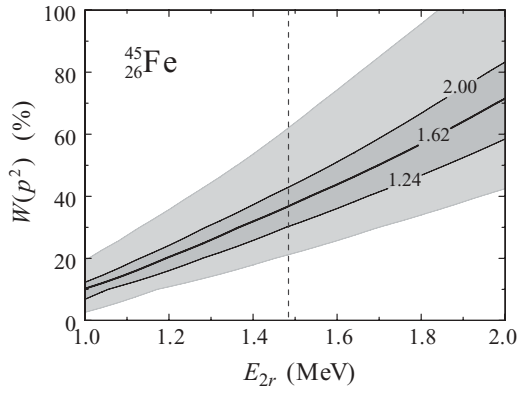

FIG. 20. Compatibility of the measured width of the ^{45}Fe with different assumptions about position E_{2r} of the ground state in the ^{44}Mn subsystem and structure of ^{45}Fe [weights of the p^2 configuration $W(p^2)$ are shown on the vertical axis]. Central gray area corresponds to experimental width uncertainty $\Gamma = (1.62 \pm 0.38) \times 10^{-19}$ MeV [12]. The light gray area also takes into account the energy uncertainty $E_{3r} = 1.154(16)$ MeV [12]. The vertical dashed line corresponds to the E_{2r} used in Fig. 19.

consistent with experimental data on the $\{E_{2r}, W(p^2)\}$ plane [$W(p^2)$ is the weight of the p^2 configuration in ^{45}Fe WF]. It is evident from this plot that our current experimental knowledge is not sufficient to draw definite conclusions. However, it is also clear that with increased precision of the lifetime and energy measurements for ^{45}Fe and the appearance of more detailed information on the ^{44}Mn subsystem, the restrictions on the theoretical models should become strong enough to provide the important structure information.

VI. DISCUSSION

General trends of the model calculations can be well understood from Tables IV–VI. For the pure Coulomb case, the simplified model calculations (in the Y and T systems) and three-body calculations provide reasonably consistent results. The simplified calculations in the Y system always give larger widths than those in the T system. From a decay dynamics point of view, this leads to an understanding of the contradictory fact that the sequential decay path is preferable also in the case where no even virtual sequential decay is possible (as the nuclear interactions are totally absent in this case).

The calculations with attractive nuclear FSIs rather expectedly provide larger widths than the corresponding calculations with Coulomb interaction only. The core-proton FSI is much more efficient for width enhancement than p-p FSI. This fact is correlated with the observation of the previous point and is a very simple and strong indication that the widespread perception of the two-proton decay as a diproton decay is misleading. As already mentioned, the p-p FSI influences the penetration strongly in the very special case when the decay occurs from high-l orbitals (e.g., f^2 in the case of ^{45}Fe). Thus we should consider as not fully consistent the attempts to explain two-proton decay results only by the FSI in the p-p channel (e.g., Ref. [19]) as a much stronger decay mechanism is neglected in these studies.

From a technical point of view, the states considered in this work belong to the most complicated cases. The complication is due to the ratio between the decay energy and the strength of the Coulomb interaction (it defines the subbarrier penetration range to be considered dynamically). Thus the convergence effects demonstrated in this work for ^{17}Ne have the strongest character among the systems studied in our previous works [4,6–8]. Because of the relatively small $K_{\max} = 12$ used in the previous works, we have found an order of the magnitude underestimation of the ^{17}Ne($3/2^-$) width. For systems like ^{48}Ni-^{66}Kr, the underestimation of widths in our previous calculations is expected to be about a factor of 2. A much smaller effect is expected for lighter systems.

It was demonstrated in Refs. [23,24] that the astrophysical radiative capture rate for the ^{15}O$(2p, \gamma)^{17}$Ne reaction depends strongly on the two-proton width of the first excited $3/2^-$ state in ^{17}Ne. This width was calculated in Ref. [7] as 4.1×10^{-16} MeV (some confusion can be connected with a misprint in Table III of Ref. [7], see Erratum [7]). However, in Ref. [21], providing very similar to Ref. [7] properties of the ^{17}Ne WFs for the ground and the lowest excited states, the width of

the $3/2^-$ state was found to be 3.6×10^{-12} MeV. It was supposed in Ref. [21] that such a strong disagreement is connected with poor subbarrier convergence of the HH method in Ref. [7] compared to the adiabatic Faddeev HH method of Ref. [21]. This point was further reiterated in Ref. [40]. We can see now that this statement has certain grounds. However, the convergence problems of the HH method are far insufficient to explain the huge disagreement: the width increase found in this work is only one order of magnitude. The most conservative upper limit $\Gamma \sim 5 \times 10^{-14}$ MeV (see Table IV) was obtained in a TFSI calculation neglecting the p-p Coulomb interaction. The other models systematically produce smaller values, with realistic calculations confined to the narrow range $\Gamma \sim (5\text{–}8) \times 10^{-15}$ MeV (Table VI). Thus the value $\Gamma \sim 4 \times 10^{-12}$ MeV obtained in Ref. [21] is very likely to be erroneous. That result is possibly connected to the simplistic quasiclassical procedure for width calculations employed in this work.

VII. CONCLUSION

In this work we derive the integral formula for the widths of the resonances decaying into the three-body channel for simplified Hamiltonians and discuss various aspects of its practical application. The basic idea of the derivation is not new, but for our specific purpose (precision solution of the multichannel problem) several important features of the scheme have not been discussed.

We can draw the following conclusions from our studies.

(i) We presume that HH convergence in realistic calculations should be largely the same as in the simplified calculations as they imitate the most important dynamic aspects of the realistic situation. The width values were somewhat underestimated in our previous calculations. The typical underestimation ranges from few percent to tens of percent for "simple" potential and from tens of percent to an order of magnitude in "complicated" cases (potentials with a repulsive core).

(ii) Convergence of the width calculations in the three-body HH model can be drastically improved by a simple adiabatic version of the Feshbach reduction procedure. For a sufficiently large dynamic sector of the basis, the calculation with effective FR potential converges from below and practically up to the exact value of the width. For a small dynamic basis, the FR calculation converges toward a width value smaller than the exact value, but still considerably improves the result.

(iii) The energy distributions obtained in the HH calculations are quite close to the exact ones. Convergence with respect to basis size is achieved at relatively small $K_{\max}$ values. The disagreement with exact distributions is not very significant and is likely to be connected not with basis size convergence but with the radial extent of the calculations [4].

(iv) The contributions of different decay mechanisms were evaluated in the simplified models. We found that the diproton decay path is much less efficient than the sequential decay path. This is true even in the model calculations without nuclear FSIs (no specific dynamics), which means that the sequential decay path is somehow kinematically preferable.

(v) The value of the width for ^{17}Ne $3/2^-$ state was underestimated in our previous work by around an order of magnitude. A very conservative upper limit is obtained in this work as $\Gamma \sim 5 \times 10^{-14}$ MeV, while typical values for realistic calculations are within the $(5\text{–}8) \times 10^{-15}$ MeV range. Thus the value $\Gamma \sim 4 \times 10^{-12}$ MeV obtained in Refs. [21,40] is likely to be erroneous.

From this paper it is clear that the convergence issue is sufficiently serious, and in some cases it was underestimated in our previous works. However, from a practical point of view, the convergence issue is not a principle problem. For example, the uncertain structure issues and subsystem properties impose typically much larger uncertainties for width values. For heavy two-proton emitters (e.g., ^{45}Fe) the positions of resonances in the subsystems are experimentally quite uncertain. For a moment this is the issue most limiting the precision of theoretical predictions. We have demonstrated that with increased precision, the experimental data impose strong restrictions on theoretical calculations, thereby allowing one to extract important structure information.

ACKNOWLEDGMENTS

The authors are grateful to Prof. K. Langanke and Prof. M. Ploszajczak for interesting discussions and to Prof. M. Pfützner for careful reading of the manuscript and corrections to the experimental data discussion. The authors acknowledge financial support from the Royal Swedish Academy of Science. L.V.G. is supported by INTAS Grants 03-51-4496 and 05-1000008-8272, Russian RFBR Grants 05-02-16404 and 05-02-17535, and Russian Ministry of Industry and Science Grant NS-8756.2006.2.

[1] V. I. Goldansky, Nucl. Phys. **19**, 482 (1960).
[2] L. V. Grigorenko, R. C. Johnson, I. G. Mukha, I. J. Thompson, and M. V. Zhukov, Phys. Rev. C **64**, 054002 (2001).
[3] L. V. Grigorenko, R. C. Johnson, I. G. Mukha, I. J. Thompson, and M. V. Zhukov, Phys. Rev. Lett. **85**, 22 (2000).
[4] L. V. Grigorenko and M. V. Zhukov, Phys. Rev. C **68**, 054005 (2003).
[5] L. V. Grigorenko, I. G. Mukha, I. J. Thompson, and M. V. Zhukov, Phys. Rev. Lett. **88**, 042502 (2002).
[6] L. V. Grigorenko, R. C. Johnson, I. G. Mukha, I. J. Thompson, and M. V. Zhukov, Eur. Phys. J. A **15**, 125 (2002).
[7] L. V. Grigorenko, I. G. Mukha, and M. V. Zhukov, Nucl. Phys. **A713**, 372 (2003); **A740**, 401(E) (2004).
[8] L. V. Grigorenko, I. G. Mukha, and M. V. Zhukov, Nucl. Phys. **A714**, 425 (2003).

[9] M. Pfutzner, E. Badura, C. Bingham, B. Blank, M. Chartier, H. Geissel, J. Giovinazzo, L. V. Grigorenko, R. Grzywacz, M. Hellstrom, Z. Janas, J. Kurcewicz, A. S. Lalleman, C. Mazzocchi, I. Mukha, G. Munzenberg, C. Plettner, E. Roeckl, K. P. Rykaczewski, K. Schmidt, R. S. Simon, M. Stanoiu, and J.-C. Thomas, Eur. Phys. J. A **14**, 279 (2002).

[10] J. Giovinazzo, B. Blank, M. Chartier, S. Czajkowski, A. Fleury, M. J. Lopez Jimenez, M. S. Pravikoff, J.-C. Thomas, F. de Oliveira Santos, M. Lewitowicz, V. Maslov, M. Stanoiu, R. Grzywacz, M. Pfutzner, C. Borcea, and B. A. Brown, Phys. Rev. Lett. **89**, 102501 (2002).

[11] B. Blank, A. Bey, G. Canchel, C. Dossat, A. Fleury, J. Giovinazzo, I. Matea, N. Adimi, F. De Oliveira, I. Stefan, G. Georgiev, S. Grevy, J. C. Thomas, C. Borcea, D. Cortina, M. Caamano, M. Stanoiu, F. Aksouh, B. A. Brown, F. C. Barker, and W. A. Richter, Phys. Rev. Lett. **94**, 232501 (2005).

[12] C. Dossat, A. Bey, B. Blank, G. Canchel, A. Fleury, J. Giovinazzo, I. Matea, F. de Oliveira Santos, G. Georgiev, S. Grèvy, I. Stefan, J. C. Thomas, N. Adimi, C. Borcea, D. Cortina Gil, M. Caamano, M. Stanoiu, F. Aksouh, B. A. Brown, and L. V. Grigorenko, Phys. Rev. C **72**, 054315 (2005).

[13] Ivan Mukha, Ernst Roeckl, Leonid Batist, Andrey Blazhev, Joachim Döring, Hubert Grawe, Leonid Grigorenko, Mark Huyse, Zenon Janas, Reinhard Kirchner, Marco La Commara, Chiara Mazzocchi, Sam L. Tabor, and Piet Van Duppen, Nature (London) **439**, 298 (2006).

[14] B. A. Brown, Phys. Rev. C **43**, R1513 (1991); **44**, 924(E) (1991).

[15] W. Nazarewicz, J. Dobaczewski, T. R. Werner, J. A. Maruhn, P.-G. Reinhard, K. Rutz, C. R. Chinn, A. S. Umar, and M. R. Strayer, Phys. Rev. C **53**, 740 (1996).

[16] F. C. Barker, Phys. Rev. C **63**, 047303 (2001).

[17] F. C. Barker, Phys. Rev. C **66**, 047603 (2002).

[18] F. C. Barker, Phys. Rev. C **68**, 054602 (2003).

[19] B. A. Brown and F. C. Barker, Phys. Rev. C **67**, 041304(R) (2003).

[20] J. Rotureau, J. Okolowicz, and M. Ploszajczak, Nucl. Phys. **A767**, 13 (2006).

[21] E. Garrido, D. V. Fedorov, and A. S. Jensen, Nucl. Phys. **A733**, 85 (2004).

[22] L. V. Grigorenko and M. V. Zhukov, Phys. Rev. C **76**, 014009 (2007).

[23] L. V. Grigorenko and M. V. Zhukov, Phys. Rev. C **72**, 015803 (2005).

[24] L. V. Grigorenko, K. Langanke, N. B. Shul'gina, and M. V. Zhukov, Phys. Lett. **B641**, 254 (2006).

[25] J. Görres, M. Wiescher, and F.-K. Thielemann, Phys. Rev. C **51**, 392 (1995).

[26] K. Nomoto, F. Thielemann, and S. Miyaji, Astron. Astrophys. **149**, 239 (1985).

[27] K. Harada and E. A. Rauscher, Phys. Rev. **169**, 818 (1968).

[28] S. G. Kadmenskii and V. E. Kalechits, Yad. Fiz. **12**, 70 (1970) [Sov. J. Nucl. Phys. **12**, 37 (1971)].

[29] S. G. Kadmensky and V. I. Furman, *Alpha-Decay and Relevant Reactions* (Energoatomizdat, Moscow, 1985) (in Russian).

[30] S. G. Kadmensky, Z. Phys. A **312**, 113 (1983).

[31] V. P. Bugrov and S. G. Kadmenskii, Sov. J. Nucl. Phys. **49**, 967 (1989).

[32] C. N. Davids, P. J. Woods, D. Seweryniak, A. A. Sonzogni, J. C. Batchelder, C. R. Bingham, T. Davinson, D. J. Henderson, R. J. Irvine, G. L. Poli, J. Uusitalo, and W. B. Walters, Phys. Rev. Lett. **80**, 1849 (1998).

[33] B. V. Danilin and M. V. Zhukov, Yad. Fiz. **56**, 67 (1993) [Phys. At. Nucl. **56**, 460 (1993)].

[34] *Handbook of Mathematical Functions*, edited by M. Abramowitz and I. Stegun (Dover Publications, New York, 1972), p. 538.

[35] I. Stefan, F. de Oliveira Santos, M. G. Pellegriti, G. Dumitru, J. C. Angelique, M. Angelique, E. Berthoumieux, A. Buta, R. Borcea, A. Coc, J. M. Daugas, T. Davinson, M. Fadil, S. Grevy, J. Kiener, A. Lefebvre-Schuhl, M. Lenhardt, M. Lewitowicz, F. Negoita, D. Pantelica, L. Perrot, O. Roig, M. G. Saint Laurent, I. Ray, O. Sorlin, M. Stanoiu, C. Stodel, V. Tatischeff, and J. C. Thomas, nucl-ex/0603020 v3.

[36] Ajzenberg-Selove, Nucl. Phys. **A460**, 1 (1986).

[37] B. V. Danilin *et al*. (unpublished).

[38] L. V. Grigorenko, Yu. L. Parfenova, and M. V. Zhukov, Phys. Rev. C **71**, 051604(R) (2005).

[39] D. Gogny, P. Pires, and R. de Tourreil, Phys. Lett. **B32**, 591 (1970).

[40] E. Garrido, D. V. Fedorov, A. S. Jensen, and H. O. U. Fynbo, Nucl. Phys. **A748**, 39 (2005).